

## THE ARECIBO GALAXY ENVIRONMENT SURVEY III: OBSERVATIONS TOWARD THE GALAXY PAIR NGC 7332/7339 AND THE ISOLATED GALAXY NGC 1156.

R. F. MINCHIN,<sup>1</sup> E. MOMJIAN,<sup>2</sup> R. AULD,<sup>3</sup> J. I. DAVIES,<sup>3</sup> D. VALLS-GABAUD,<sup>4</sup> I. D. KARACHENTSEV,<sup>5</sup> P. A. HENNING,<sup>6</sup> K. L. O'NEIL,<sup>7</sup> S. SCHNEIDER,<sup>8</sup> M. W. L. SMITH,<sup>3</sup> M. D. STAGE,<sup>8</sup> R. TAYLOR,<sup>3</sup> AND W. VAN DRIEL<sup>4</sup>

*Draft version November 8, 2018*

### ABSTRACT

Two 5 square degree regions around the NGC 7332/9 galaxy pair and the isolated galaxy NGC 1156 have been mapped in the 21-cm line of neutral hydrogen (H I) with the Arecibo L-band Feed Array out to a redshift of  $\sim 0.065$  ( $\sim 20000$  km s<sup>-1</sup>) as part of the Arecibo Galaxy Environment Survey. One of the aims of this survey is to investigate the environment of galaxies by identifying dwarf companions and interaction remnants; both of these areas provide the potential for such discoveries. The neutral hydrogen observations were complemented by optical and radio follow-up observations with a number of telescopes. A total of 87 galaxies were found, of which 39 (45 per cent) were previously cataloged and 15 (17 per cent) have prior redshifts. Two dwarf galaxies have been discovered in the NGC 7332 group and a single dwarf galaxy in the vicinity NGC 1156. A parallel optical search of the area revealed one further possible dwarf galaxy near NGC 7332.

*Subject headings:* galaxies: individual (NGC 7332) – galaxies: individual (NGC 7339) – galaxies: individual (NGC 1156) – radio lines: galaxies – surveys

### 1. INTRODUCTION

The NGC 7332 and NGC 1156 regions are the first two completely surveyed areas from the Arecibo Galaxy Environment Survey (AGES). The survey aims to address a number of scientific goals, including the H I mass function in different environments, the contribution of neutral gas to the baryonic mass density, the identification of gaseous tidal features, and the identification of isolated neutral gas clouds. In order to do this, AGES is investigating galaxies in a number of different environments, from the Local Void through to the Virgo Cluster. These environments include three isolated galaxies (NGC 1156, described here, UGC 2082, and NGC 5233) and two galaxy pairs (NGC 7332/9, described here, and NGC 2577/UGC 4375). A full description of the aims of the survey, which is expected to be concluded in around four to five years, can be found in Auld et al. (2006) and on the AGES website<sup>1</sup>.

#### 1.1. *The NGC 7332 region*

NGC 7332 and NGC 7339 form a close pair (5.2 arc minutes separation) with velocities of 1172 and 1313 km s<sup>-1</sup> respectively. They lie at a distance of 23 Mpc (Tonry et al. 2001, from surface-brightness fluctuations), giving a projected separation of 35 kpc. We adopt the Tonry et al. distance throughout this paper and convert masses and fluxes from the literature to this distance.

NGC 7332 itself is an S0 galaxy; whether or not it contains neutral hydrogen has been debated in the literature for many years. Knapp, Kerr & Williams (1978), using Arecibo with the circular-polarised L-band feed (FWHM  $3.3 \pm 0.1$  arcmin), claimed a detection with an H I mass  $1.1 \times 10^8 M_{\odot}$ . Biermann, Clarke & Fricke (1979), using the same receiver, also see this signal but attribute it to side-lobe contamination from NGC 7339. Haynes

(1981) and Burstein, Krumm & Salpeter (1987) both observed the galaxy using Arecibo with the linear-polarised L-band feed (FWHM  $3.9 \pm 0.1$  arcmin), which had significantly lower side-lobes than the circular-polarised feed but also less sensitivity ( $6$  K Jy<sup>-1</sup> versus  $8$  K Jy<sup>-1</sup>), and Balkowski & Chamaraux (1983) observed it with the Nançay Radio Telescope (FWHM  $4 \times 22$  arcmin). None of these observations had the sensitivity to detect the signal seen by Knapp et al., although Haynes (1983) discusses the Knapp et al. detection and attributes it to side-lobes.

Ionized hydrogen has been detected in NGC 7332 (Plana & Boulesteix 1996) which extends over the velocity range of the Knapp et al. neutral hydrogen detection. This ionized gas is organised into two dynamically separate discs, one of which (the more massive) is counter-rotating with respect to the stars.

The ionized gas in NGC 7332 was also examined by Falcón-Barroso et al. (2004). They found that “NGC 7332 is young everywhere” and that there was “a significant amount of unsettled gas”, suggesting that “NGC 7332 is still evolving”. Both Falcón-Barroso et al. and Plana & Boulesteix find that a recent accretion event is the likely source of the counter-rotating gas disc. Falcón-Barroso et al. also suggest that the same event could have led to the formation of the bar in this galaxy, and that later accretion may be required to explain some other features of the ionized gas distribution.

Morganti et al. (2006) observed NGC 7332 with the Westerbork Synthesis Radio Telescope (WSRT). They did not detect any gas at the position of NGC 7332 but did detect the gas in NGC 7339 and also found a cloud with an H I mass of  $6 \times 10^6 M_{\odot}$  around 3 arc minutes from NGC 7332, in the direction of NGC 7339, which they attribute to an interaction between the two galaxies.

NGC 7339 is a nearly edge-on Sbc galaxy. It has been observed a number of times in the H I line. Springob et al. (2005) find a neutral hydrogen mass of  $1.3 \times 10^9 M_{\odot}$  after

<sup>1</sup> <http://www.naic.edu/~ages>

correction for the size of the galaxy, which is consistent with the mass of  $1.2 \pm 0.2 \times 10^9 M_\odot$  found by Staveley-Smith & Davies (1987) with the Lovell Telescope at Jodrell Bank.

Besides the two giant galaxies, two dwarf spheroidal galaxies, KKR 72 and KKR 73, have been noted by Karachentseva, Karachentsev & Richter (1999) as being possibly associated with the group following a careful search of POSS II films. Attempts to observe HI in these galaxies by Huchtmeier, Karachentsev & Karachentseva (2000) reached a limit of around  $10^8 M_\odot$  but did not detect anything.

The region behind NGC 7332 is poorly studied. There are only nine redshifts for galaxies in NED<sup>2</sup>. Directly behind NGC 7332 lie a succession of void regions, identified by Fairall (1998) as parts of the Delphinus, Cygnus and Pegasus voids. The AGES region lies within, but close to the edge of, these voids out to  $\sim 7000 \text{ km s}^{-1}$ .

The survey area of  $2.5^\circ \times 2^\circ$  equates to a physical area of  $0.8 \text{ Mpc}^2$  at the distance of NGC 7332, allowing us to see a wide region around the galaxy pair. AGES observations of this region are particularly motivated by the possibility of finding interaction remnants from NGC 7332 and NGC 7339 along with searching their local environment for dwarf galaxies.

### 1.2. The NGC 1156 region

NGC 1156 is a nearby, star-forming, irregular galaxy at a redshift of  $375 \text{ km s}^{-1}$ . It is similar in both optical appearance and HI mass to the Large Magellanic Cloud. The galaxy is listed in the isolated galaxy catalogue of Karachentseva, Lebedev & Shcherbanovskij (1973) as one of the most isolated galaxies in the nearby Universe, with no companion within  $10^\circ$ . Karachentsev, Musella & Grimaldi (1996) estimated its distance as 7.8 Mpc (on the basis of the brightest stars); we have adopted this estimate in this paper. The nearest significant companion (taken to be one with at least 10 per cent of the  $B$ -band luminosity) is UGC 2259 which lies at an angular separation of 12.5 degrees and a distance from Earth of 10 Mpc (Tully & Fisher 1988), giving it a  $B$ -band luminosity of 11 per cent of NGC 1156 and a distance from NGC 1156 of 2.9 Mpc. The closest galaxy of a similar or larger size (one with at least 50 per cent of the  $B$ -band luminosity) is NGC 1023 at an angular separation of 14.4 degrees and a distance from Earth of 10.4 Mpc (Ajhar et al. 1997), giving it a  $B$ -band luminosity around 400 times larger than NGC 1156 and a distance from NGC 1156 of 3.4 Mpc.

A number of studies have included the galaxy, due to its isolation and its status as a relatively close, irregular galaxy with fairly active star formation. Relevant data from these studies is described below.

Swaters et al. (2002) observed NGC 1156 with the WSRT as part of the WHISP (Westerbork HI Survey of Spiral and Irregular Galaxies) project. These data show a clumpy HI morphology at small scales, with holes and knots particularly visible in the outskirts, and possible signs of a warp in the central regions. Swa-

ters et al. found an HI flux of  $71.3 \text{ Jy km s}^{-1}$ , giving  $M_{\text{HI}} = 1.02 \times 10^9 M_\odot$ . This is consistent with the  $71.27 \text{ Jy km s}^{-1}$  Green Bank 43-m measurement of Haynes et al. (1998) which, with a beam-size of 21 arcminutes, should not resolve the galaxy. Haynes et al. estimate a finite source size correction of 2 per cent for their NGC 1156 measurement, giving a final flux of  $72.72 \text{ Jy km s}^{-1}$ .

Barazza, Binggelli & Prugniel (2001) included NGC 1156 in their sample of nearby field galaxies. They measured an extinction-corrected  $B$  magnitude of  $11.78 \pm 0.10$  and extinction-corrected colors of  $B - V = 0.46$  and  $B - R = 0.87$ . This gives an absolute  $B$  magnitude of  $-17.68$  and an HI mass to light ratio (using the Swaters et al. HI mass) of  $M_{\text{HI}}/L_B = 0.56 M_\odot/L_\odot$ , which is fairly typical for a Magellanic irregular.

NGC 1156 was included in the sample of galaxies studied in H $\alpha$  by James et al. (2004). They found an  $R$ -band magnitude of  $11.91 \pm 0.04$  (uncorrected for extinction), and a star formation rate (using our adopted distance of 7.8 Mpc) of  $0.71 \pm 0.07 M_\odot \text{ yr}^{-1}$ .

The kinematics of NGC 1156 were studied in detail by Hunter et al. (2002) as part of a study of star-forming irregular galaxies. They found that the kinematical axes of the ionized gas, neutral gas and stellar discs were probably aligned at a position angle of  $84^\circ$ . This is markedly different from the morphological position angle of  $39^\circ$ , due to the light of the galaxy being dominated by its bar. In the HI, they report a structure resembling a tiny tidal tail to the north-east of the galaxy, terminating in an HI complex with a large velocity width.

The background region behind NGC 1156 passes through the outskirts of the Taurus void (Fairall 1998). It is only marginally better studied than the NGC 7332 region, with 12 redshifts in NED (not including NGC 1156 itself), many of them from the Springob et al. (2005) Arecibo General Catalog. Two groups have been identified at just over  $10\,000 \text{ km s}^{-1}$ : WBL 091 (White et al. 1999) and PPS2 187 (Trasarti-Battistoni 1998).

The AGES observations of the NGC 1156 region cover an area of  $2.5^\circ \times 2^\circ$ , equivalent to  $0.09 \text{ Mpc}^2$  at the distance of NGC 1156. The observations are particularly motivated by the possibility of finding low surface-brightness companions and dwarf galaxies that have evaded optical detection but that may have interacted (or even be interacting) with NGC 1156.

## 2. OBSERVATIONS AND DATA REDUCTION

The HI survey observations of the NGC 1156 region were carried out using the 305-m telescope at Arecibo Observatory<sup>3</sup> between December 2005 and February 2006 and those of the NGC 7332 region between July and September, 2006. Both sets of observations used the Arecibo L-band Feed Array multibeam system<sup>4</sup> and the fixed-azimuth drift observing mode to reach an integration time of around  $300 \text{ s point}^{-1}$ . The data reduction used the standard AGES pipeline (Cortese et al. 2008), which is based on that used for HIPASS (Barnes et al. 2001) and uses the Livedata and Gridzilla multibeam processing packages<sup>5</sup>. Baseline estimation and calibra-

<sup>3</sup> Arecibo Observatory is part of the National Astronomy and Ionosphere Center, which is operated by Cornell University under a cooperative agreement with the NSF.

<sup>4</sup> see <http://www.naic.edu/alfa> for more details

<sup>5</sup> <http://www.atnf.csiro.au/computing/software/livedata.html>

<sup>2</sup> The NASA/IPAC Extragalactic Database (NED) is operated by the Jet Propulsion Laboratory, California Institute of Technology, under contract with the National Aeronautics and Space Administration.

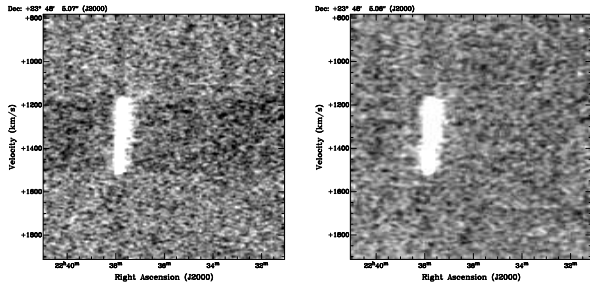


FIG. 1.— Comparison between the standard (left) and extended-source optimised (right) cubes, showing NGC 7339. Both have been Hanning smoothed and show the same R.A.-velocity slice through the NGC 7332 cube, clipped at equivalent  $3\sigma$  levels. It can be seen that the standard cube has a ‘shadow’ in the scan direction, which has removed flux from NGC 7339. This is not present in the extended-source optimised cube.

tion were carried out using Livedata, which estimates the baseline to be removed by median combining an entire drift scan, and the reduced spectra were gridded into a datacube using Gridzilla.

The reduced data cubes were Hanning-smoothed with a width of three channels, giving a velocity resolution of  $10 \text{ km s}^{-1}$  and a noise of  $0.75 \text{ mJy channel}^{-1} \text{ beam}^{-1}$ . The final beam resolution (from 2-D Gaussian fitting on the  $670 \text{ mJy}$  continuum source  $4C +24.59$  which is close to NGC 7332; Condon et al. 1998) was 3.4 arc minutes (the same as the input beam).

### 2.1. Extended Sources

The standard AGES pipeline is optimized for point sources and, as such, does not give the correct flux for extended sources such as NGC 7339 (in the NGC 7332 field) and NGC 1156. There are two reasons for this: firstly the baseline estimation carried out in Livedata can remove flux if a strong source fills a significant portion of a scan and secondly the gridding is optimised to correctly reconstruct the flux of a point-source at the pixel center.

In order to overcome this problem, we have formed a extended-source cubes of the regions around NGC 1156 and NGC 7332 using the MinMed bandpass estimator in Livedata (Putman et al. 2002) and without applying the beam normalization in Gridzilla. This gives a reduction in the flux of point sources but gives correct fluxes for gas that overfills the beam. Following Hanning smoothing, the noise in the extended-source cubes was  $0.4 \text{ mJy beam}^{-1}$  for the NGC 7332 and  $0.7 \text{ mJy beam}^{-1}$  for NGC 1156 (implying that the bandpass estimate from MinMed was not as effective for NGC 1156 as for NGC 7332). The gridded beam remained at 3.4 arc minutes, giving a  $3\sigma$  sensitivity to extended emission that fills or overfills the beam of  $5 \times 10^{17} (\Delta V/10) \text{ atoms cm}^{-2}$  in NGC 7332 and  $8 \times 10^{17} (\Delta V/10) \text{ atoms cm}^{-2}$  in NGC 1156.

The difference between the standard and extended cubes can be seen in Fig. 1. The standard cube has a ‘shadow’ in the scan direction (R.A.) caused by NGC 7332 being included in the determination of the baseline. This causes the extension of NGC 7332 in the R.A. direction to be visibly truncated on the standard cube as well as removing flux from the whole galaxy.

The fluxes of the extended sources (NGC 7339 and NGC 1156) were found by fitting a 2D Gaussian (using the MIRIAD routine IMFIT to a moment 0 map of each source made from the relevant extended-source optimised

cube. The measured flux was then beam-corrected using a size for the beam of 3.4 arc minutes. In addition to the flux, this method fits the position, deconvolved size, and position angle of the source. As described in the sections on NGC 7339 and NGC 1156, this gives an estimate of the flux of these galaxies that is consistent with previous measurements. The spectral parameters of the extended sources were measured on summed and beam-corrected spectra formed in an 11 by 11 arc minute box, also on the extended-source optimised cubes

### 2.2. Radio Frequency Interference

The survey data is affected by radio frequency interference (RFI) at 1350 MHz from the Federal Aviation Authority radar at Pico del Este. This is seen at  $\sim 15000 \text{ km s}^{-1}$ . An intermod of the Punta Salinas radar at 1241.7 MHz appears in the data at  $\sim 7000 \text{ km s}^{-1}$ . As these radar signals are present in all or nearly all of the observations, they are not removed by median combining the data.

The other major source of RFI is the GPS L3 beacon at 1380 MHz, which is seen at  $\sim 8800 \text{ km s}^{-1}$  in the data. However, this only transmits intermittently and is therefore mostly removed when the data are combined. Extra care is taken when identifying previously uncatalogued sources at this redshift to ensure that they are true HI sources and not GPS transmissions.

## 3. THE AGES CATALOG

The NGC 7332 cube was searched independently by eye by two members of the team (RM & EM). Detections were classified as ‘solid’ or ‘dubious’. Any detections not classified as ‘solid’ by both searchers were targeted for follow-up observations. These were carried out with the L-Band Wide and ALFA receivers at Arecibo Observatory during the summer of 2008.

The NGC 1156 cube was searched by two members of the team (RA & Luca Cortese) and using an automated searching algorithm (see Cortese et al. 2008 for details). Any detections with a signal to noise of less than 7 (calculated retrospectively from the measured parameters, see below for details) were followed up with the L-band Wide receiver at Arecibo Observatory during the winter of 2006 and the fall of 2009.

All of the sources in the catalog presented here (Table 1) are either therefore considered solid detections on the original AGES cubes or have been confirmed by follow-up observations. The data is presented in the same format as Cortese et al. (2008): Column 1 gives the AGES HI source ID. Columns 2 and 3 give the right ascension of the HI source and its associated error (in seconds of right ascension). Columns 3 and 4 give the declination of the HI source and its associated error (in seconds of arc). Column 6 gives the heliocentric velocity ( $cz$ ) and associated error, measured as the mid-point of the HI profile at 50 per cent of the peak flux. Columns 7 and 8 give the observed width of the HI profile (not corrected for instrumental broadening, turbulent motions, etc.) at 50 and 20 per cent respectively of the peak flux, along with their associated errors. Column 9 gives the peak flux density and its associated error. Column 10 gives the integrated flux and its associated error. Column 11 gives the object flags, defined as follows: flag 0 is a source securely detected in the survey data; flag 1 is a source confirmed by

follow-up observations; flag 2 is a source contaminated by RFI (none of the sources in the regions reported in this paper have this flag); flag 3 marks extended sources, measured as described in Section 2.1.

The HI parameters in Table 1 were derived as in Cortese et al. 2008 using the MIRIAD routine MBSPECT. Uncertainties were derived using the equations from Koribalski et al. (2004), e.g.  $\sigma(F_{HI}) = 4 \times (\sigma(S_{peak})/S_{peak}) \times (S_{peak} F_{HI} \delta v)^{1/2}$ , where  $\delta v$  is the channel width and  $\sigma(S_{peak})$  is taken to be the quadrature sum of the rms measured off-source and  $0.05 S_{peak}$ , e.g.  $\sigma(S_{peak})^2 = rms^2 + (0.05 S_{peak})^2$ . The uncertainty in the systematic velocity is given by  $\sigma(V = 3 \times \sigma(S_{peak})/S_{peak} \times (\frac{W_{50}-W_{20}}{2} \delta v)^{1/2})$ ; errors in the widths are given by  $\sigma(W_{50} = 2\sigma(V))$  and  $\sigma(W_{20} = 3\sigma(V))$ . The positions and their associated errors are from the fitting of a gaussian to the source in MBSPECT, the errors are the formal errors on the fit and, while they are indicative of the quality of the fit, do not correspond directly to the offset between the HI position and the optical position and appear to underestimate the true uncertainty in the position by a factor of around three (see Section 5.3).

Following Giovanelli et al. (2005), Cortese et al. (2008), Kent et al. (2009) and Henning et al. (2010), we characterise the effective signal to noise ratio of the galaxies retrospectively using the measured parameters on sources originally detected by-eye. The SNR is estimated as:

$$SNR = \frac{F_{HI}}{\sigma} \sqrt{\frac{\omega}{20}} \frac{1}{W_{50}} \quad (1)$$

Where  $\omega = W_{50}$  (the velocity width at 50 per cent of the peak height) for  $W_{50} < 400 \text{ km s}^{-1}$  and  $\omega = 400 \text{ km s}^{-1}$  for higher velocity widths. This corresponds to optimal selection ( $\propto 1/\sqrt{\Delta V}$ ) at lower velocity widths and peak-flux selection at higher velocity widths. We find that most of our data fall above an approximate detection limit of  $SNR = 5$ , as can be seen in Fig. 3. Fig. 4 shows how the sensitivity (in terms of detectable HI mass) varies with distance. Both also give the ALFALFA limit for comparison purposes (note that ALFALFA and AGES do not use entirely consistent definitions of  $W_{50}$ , so this limit is necessarily only an approximation).

#### 4. FOLLOW-UP OBSERVATIONS

##### 4.1. L-band Follow-up Observations

A number of sources that were not secure detections in the AGES cubes were confirmed by follow-up observations. NGC 1156 sources were followed up in October 2006 with the L-Band Wide (LBW) receiver using the Interim Correlator (IC) backend and in September 2009 with the same receiver using the WAPP backend. NGC 7332 sources were followed up in July to September 2008 using either the L-Band Wide receiver or the central pixel of ALFA, both using the WAPP backend. The observations are summarised in Table 2. The AGES ID matches the catalog AGES ID for confirmed sources, for unconfirmed sources it is merely indicative – these ‘sources’ are most probably noise fluctuations or baseline ripples introduced by continuum sources. ‘No. obs.’ indicates the number of 300s on-source on-off observations that were

made of the source. The RA and Dec given here are the targetted RA and Dec and the velocity is the targetted central velocity. These may not always match precisely with the cataloged RA, Dec and central velocity (Table 1).

All observations were on-off observations with 300s on-source integration time. Data reduction was performed using the standard routines in the AO-IDL system. The data were smoothed to the same resolution as AGES survey observations ( $10 \text{ km s}^{-1}$ ) and reach noise levels of around  $0.7 \text{ mJy}$ . Multiple observations were carried out on sources which showed a possible signal at the location that was too weak to call a confirmation, this was often due to the presence of continuum radiation causing baseline ripple and increased noise levels.

The confirmation rate for follow-up on the NGC 1156 field was 28 per cent (7 out of 25), while the confirmation rate on the NGC 7332 field was substantially higher, at 74 per cent (17 out of 23), similar to the confirmation rate in the NGC 1156 field (Cortese et al. 2008). This is due to the difference in the selection criteria for follow-up observations used in the two fields (see §3) – these were changed after most of the follow-up of NGC 1156 had been completed and continue to be modified in order to make the most efficient use of follow-up time.

##### 4.2. Optical survey of the NGC 7332 region

In addition to the neutral hydrogen observations, we have carried out a careful search of the blue and red POSS-II plates within 300 kpc (45 arc minutes) of NGC 7332. This repeated the search of Karachentseva et al. (1999) but included galaxies with a smaller diameter to account for the group being at 23 Mpc while Karachentseva et al. were primarily searching for objects within 10 Mpc. This search turned up a further three candidate dwarf galaxies: J223450+240757 lies 41 arc minutes from NGC 7332 and appears to be a background galaxy although it could be a dIrr, J223558+234825 is 20 arc minutes away and has the appearance of a dSph, while J223631+240814 is 13 arc minutes away and also appears to be a dSph.

On cross-referencing this with the main AGES source list, it became apparent that J223450+240757 and J223631+240814 were background galaxies. We therefore add one candidate dSph, J223558+234825, to the list of possible group members.

##### 4.3. Optical spectroscopy

Optical redshifts were obtained for a number of galaxies in the NGC 1156 and NGC 7332 regions using a dispersion grism on the 1.5-m telescope at Loiano Observatory. Data reduction was carried out in IRAF. The frames were bias-subtracted and flat-fielded and spectral calibration was carried out using a template spectrum from an Ar-He lamp. No flux calibration was applied. Post-calibration, the data were sky subtracted to minimise the impact of night sky lines. A final 1-D spectrum was produced by integrating over pixels that appeared to contain emission from the target galaxy. The results of these observations are given in Table 3, along with the AGES HI velocities for these galaxies.

##### 4.4. VLA observations of AGES J224005+244154

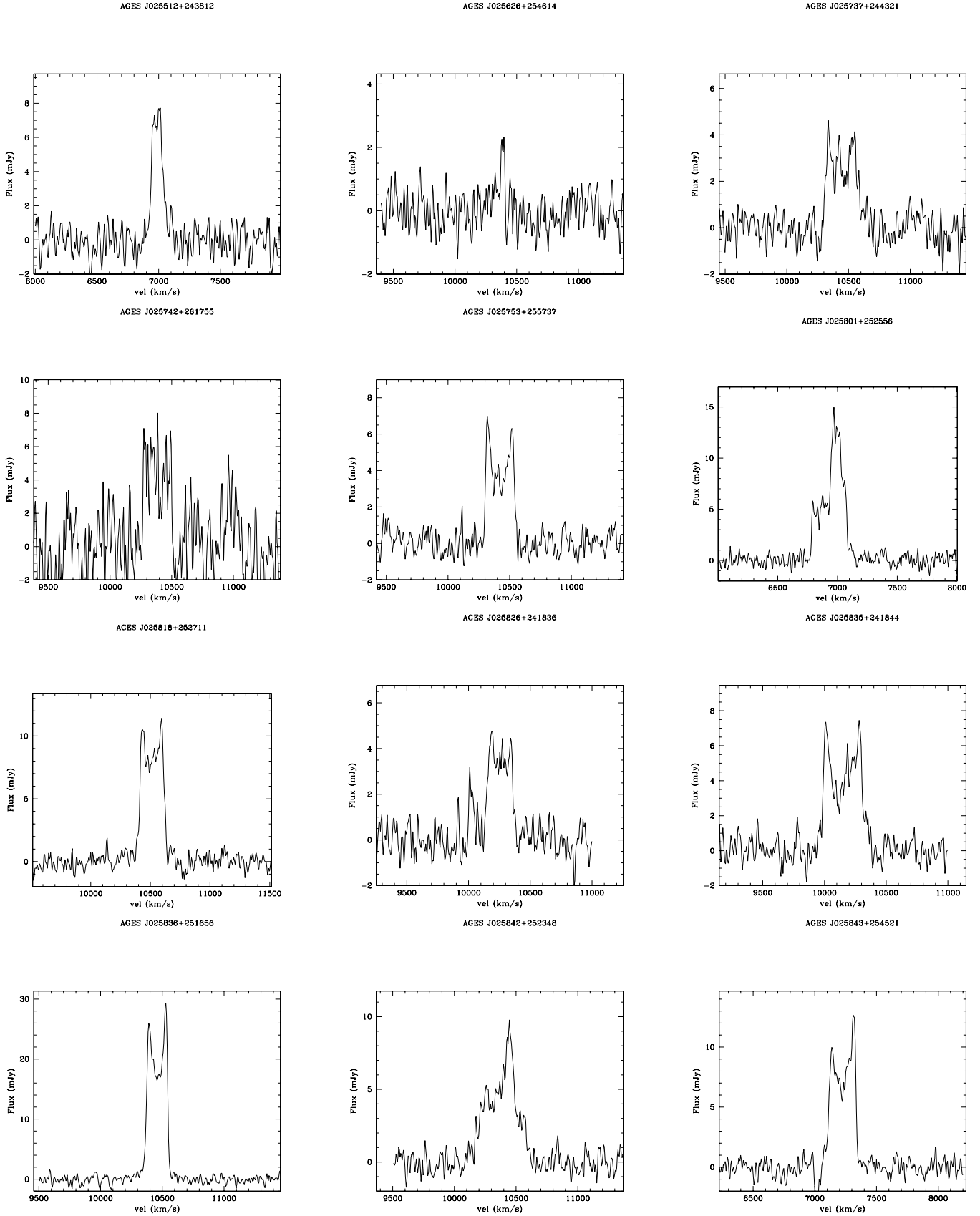


FIG. 2.— Spectra of sources from the NGC 1156 and NGC 7332 regions. Only the first page is shown due to ArXiv size constraints - please see the journal version for the full figure.

TABLE 1  
 HI PROPERTIES OF THE AGES GALAXIES IN THE NGC 7332 AND NGC 1156 REGIONS.

HI ID	R.A. (J2000)	$\sigma_{R.A}$ (s)	Dec. (J2000)	$\sigma_{Dec.}$ (arc sec)	V (km s <sup>-1</sup> )	W50 (km s <sup>-1</sup> )	W20 (km s <sup>-1</sup> )	$S_{Peak}$ (mJy)	$F_{HI}$ (Jy km s <sup>-1</sup> )	Flag
AGES J025512+243812	02:55:11.9	1.1	24:38:12	19	6988 ± 6	98 ± 12	180 ± 18	8.0 ± 0.8	0.679 ± 0.094	0
AGES J025626+254614	02:56:26.0	1.4	25:46:14	14	10364 ± 7	80 ± 15	107 ± 22	2.4 ± 0.5	0.080 ± 0.037	1
AGES J025737+244321	02:57:36.5	0.7	24:43:21	12	10452 ± 11	265 ± 21	434 ± 32	4.5 ± 0.5	0.824 ± 0.094	0
AGES J025742+261755	02:57:42.4	0.8	26:17:55	12	10383 ± 4	231 ± 8	239 ± 12	7.9 ± 1.6	1.093 ± 0.245	1
AGES J025753+255737	02:57:53.2	0.7	25:57:37	11	10421 ± 3	234 ± 5	254 ± 8	6.9 ± 0.6	1.088 ± 0.097	0
AGES J025801+252556	02:58:00.7	0.7	25:25:56	12	7002 ± 5	125 ± 11	298 ± 16	15.4 ± 0.9	1.936 ± 0.130	0
AGES J025818+252711	02:58:17.6	0.7	25:27:11	11	10514 ± 2	204 ± 5	233 ± 7	12.5 ± 0.8	1.956 ± 0.127	0
AGES J025826+241836	02:58:25.6	2.3	24:18:36	13	10254 ± 7	208 ± 14	274 ± 21	5.2 ± 0.7	0.815 ± 0.104	0
AGES J025835+241844	02:58:34.8	0.7	24:18:44	10	10147 ± 5	317 ± 10	394 ± 15	7.0 ± 0.6	1.678 ± 0.119	0
AGES J025836+251656	02:58:35.5	0.7	25:16:56	10	10459 ± 2	171 ± 3	191 ± 5	30.2 ± 1.6	3.866 ± 0.228	0
AGES J025842+252348	02:58:42.2	1.3	25:23:48	29	10369 ± 7	236 ± 15	415 ± 22	9.2 ± 0.8	1.854 ± 0.136	0
AGES J025843+254521	02:58:42.6	0.7	25:45:21	10	7225 ± 2	218 ± 4	239 ± 6	12.8 ± 0.8	1.955 ± 0.127	0
AGES J025902+253518	02:59:01.8	1.2	25:35:18	13	7176 ± 10	272 ± 19	354 ± 29	3.3 ± 0.5	0.262 ± 0.059	1
AGES J025917+244756	02:59:17.4	0.9	24:47:56	12	4658 ± 3	56 ± 6	77 ± 8	6.7 ± 0.6	0.342 ± 0.054	0
AGES J025930+255419	02:59:30.3	0.7	25:54:19	14	10407 ± 7	221 ± 13	306 ± 20	5.2 ± 0.6	0.928 ± 0.095	0
AGES J025936+253446	02:59:36.0	0.8	25:34:46	11	10253 ± 7	68 ± 15	125 ± 22	3.6 ± 0.5	0.216 ± 0.052	1
AGES J025942+251430	02:59:42.3	0.7	25:14:30	10	379 ± 2	75 ± 4	113 ± 6	925.0 ± 46.3	75.6 ± 6.4	3
AGES J025953+254350	02:59:53.0	0.8	25:43:50	13	7192 ± 11	19 ± 23	117 ± 34	3.1 ± 0.5	0.114 ± 0.040	0
AGES J025954+241323	02:59:54.1	0.7	24:13:23	10	10224 ± 2	303 ± 5	329 ± 7	15.8 ± 1.1	3.302 ± 0.193	0
AGES J030008+241600	03:00:08.3	0.7	24:16:00	10	15081 ± 5	430 ± 10	441 ± 15	6.2 ± 1.4	1.483 ± 0.280	0
AGES J030014+250315	03:00:14.0	0.7	25:03:15	10	11308 ± 2	76 ± 4	92 ± 7	7.7 ± 0.6	0.492 ± 0.064	0
AGES J030025+255335	03:00:24.9	0.7	25:53:35	15	10612 ± 5	104 ± 9	111 ± 14	2.3 ± 0.6	0.169 ± 0.066	1
AGES J030027+241301	03:00:27.2	0.8	24:13:01	10	9877 ± 5	57 ± 10	170 ± 14	15.4 ± 1.0	0.933 ± 0.102	0
AGES J030036+241156	03:00:36.4	1.1	24:11:56	11	15183 ± 9	112 ± 17	158 ± 26	4.9 ± 0.9	0.427 ± 0.110	1
AGES J030039+254656	03:00:39.3	1.6	25:46:56	15	308 ± 3	19 ± 7	44 ± 10	5.8 ± 0.6	0.114 ± 0.032	0
AGES J030112+242411	03:01:11.5	0.7	24:24:11	10	9781 ± 4	392 ± 7	429 ± 11	6.8 ± 0.6	1.594 ± 0.117	0
AGES J030136+245602	03:01:36.1	0.7	24:56:02	11	10417 ± 8	188 ± 16	243 ± 24	3.3 ± 0.5	0.366 ± 0.070	0
AGES J030139+254442	03:01:39.2	0.7	25:44:42	13	6722 ± 4	149 ± 7	187 ± 11	7.0 ± 0.6	0.952 ± 0.090	0
AGES J030146+254314	03:01:45.8	0.8	25:43:14	14	11216 ± 3	312 ± 6	332 ± 8	6.5 ± 0.6	1.378 ± 0.110	0
AGES J030200+250030	03:01:59.7	0.7	25:00:30	11	7025 ± 2	264 ± 5	286 ± 7	9.2 ± 0.7	1.808 ± 0.120	0
AGES J030204+254745	03:02:04.0	0.7	25:47:45	10	6791 ± 3	253 ± 6	280 ± 9	7.4 ± 0.6	1.421 ± 0.109	0
AGES J030234+244938	03:02:34.1	0.7	24:49:38	10	3260 ± 1	48 ± 3	63 ± 4	22.4 ± 1.2	0.983 ± 0.103	0
AGES J030254+260028	03:02:54.2	0.7	26:00:28	10	10625 ± 2	117 ± 4	135 ± 5	13.9 ± 0.9	1.555 ± 0.114	0
AGES J030309+260407	03:03:08.6	0.7	26:04:07	11	14014 ± 9	209 ± 18	281 ± 27	3.4 ± 0.5	0.433 ± 0.075	0
AGES J030325+241510	03:03:25.3	0.7	24:15:10	11	14750 ± 8	158 ± 17	292 ± 25	7.4 ± 0.8	0.933 ± 0.112	0
AGES J030355+241922	03:03:54.7	0.7	24:19:22	12	14517 ± 11	102 ± 23	286 ± 34	5.3 ± 0.7	0.496 ± 0.080	0
AGES J030450+260045	03:04:50.3	0.8	26:00:45	11	9424 ± 10	134 ± 20	183 ± 31	2.9 ± 0.6	0.239 ± 0.071	1
AGES J030453+251532	03:04:53.1	0.7	25:15:32	10	14206 ± 5	239 ± 10	267 ± 16	5.1 ± 0.7	0.735 ± 0.113	0

TABLE 1  
(CONTINUED)

HI ID	R.A. (J2000)	$\sigma_{R.A}$ (s)	Dec. (J2000)	$\sigma_{Dec.}$ (arc sec)	V (km s <sup>-1</sup> )	W50 (km s <sup>-1</sup> )	W20 (km s <sup>-1</sup> )	$S_{Peak}$ (mJy)	$F_{HI}$ (Jy km s <sup>-1</sup> )	Flag
AGES J223111+234146	22:31:11.0	0.7	23:41:46	14	16645 ± 3	266 ± 7	276 ± 10	3.9 ± 0.6	0.491 ± 0.090	1
AGES J223122+230436	22:31:22.1	0.7	23:04:36	10	17017 ± 3	200 ± 7	214 ± 10	5.7 ± 0.8	0.692 ± 0.105	0
AGES J223143+244513	22:31:43.0	0.7	24:45:13	13	16130 ± 7	167 ± 13	233 ± 20	4.5 ± 0.5	0.565 ± 0.078	1
AGES J223213+232657	22:32:12.6	0.7	23:26:57	10	16892 ± 3	160 ± 7	193 ± 10	8.6 ± 0.7	1.226 ± 0.111	0
AGES J223218+235131	22:32:17.8	0.7	23:51:31	10	11950 ± 6	367 ± 12	403 ± 18	3.6 ± 0.5	0.731 ± 0.096	0
AGES J223223+232613	22:32:23.4	0.7	23:26:13	10	11427 ± 8	51 ± 16	288 ± 24	9.8 ± 0.8	0.727 ± 0.084	0
AGES J223231+231601	22:32:30.5	0.8	23:16:01	11	11787 ± 10	361 ± 20	475 ± 31	3.7 ± 0.5	0.902 ± 0.105	1
AGES J223236+235555	22:32:36.3	0.7	23:55:55	10	7457 ± 2	329 ± 4	349 ± 6	11.3 ± 0.8	2.628 ± 0.146	0
AGES J223237+231209	22:32:37.2	0.7	23:12:09	11	16614 ± 6	209 ± 11	236 ± 17	3.2 ± 0.5	0.444 ± 0.079	1
AGES J223245+243816	22:32:45.2	0.7	24:38:16	11	15968 ± 8	117 ± 16	199 ± 23	5.1 ± 0.7	0.515 ± 0.083	0
AGES J223318+244545	22:33:17.8	0.8	24:45:45	11	12232 ± 4	450 ± 8	462 ± 12	4.3 ± 0.7	0.946 ± 0.137	1
AGES J223320+230400	22:33:20.2	0.7	23:04:00	10	7623 ± 4	92 ± 8	125 ± 12	5.4 ± 0.6	0.476 ± 0.068	0
AGES J223329+231109	22:33:29.1	0.7	23:11:09	10	13600 ± 6	187 ± 11	248 ± 17	6.3 ± 0.7	0.930 ± 0.104	0
AGES J223342+242712	22:33:42.1	0.8	24:27:12	11	9975 ± 5	130 ± 10	184 ± 15	5.8 ± 0.6	0.687 ± 0.079	0
AGES J223355+243114	22:33:54.9	0.9	24:31:14	22	10012 ± 4	115 ± 9	132 ± 13	3.4 ± 0.5	0.265 ± 0.059	1
AGES J223415+233057	22:34:15.0	0.8	23:30:57	12	16476 ± 8	136 ± 15	186 ± 23	3.3 ± 0.5	0.370 ± 0.070	1
AGES J223449+240744	22:34:48.8	0.7	24:07:44	12	16289 ± 2	40 ± 5	58 ± 7	8.9 ± 0.7	0.315 ± 0.056	0
AGES J223502+235258	22:35:01.7	0.7	23:52:58	11	9713 ± 8	151 ± 16	192 ± 23	2.9 ± 0.5	0.255 ± 0.062	1
AGES J223502+242131	22:35:02.4	0.7	24:21:31	12	12241 ± 9	170 ± 18	235 ± 28	3.1 ± 0.5	0.332 ± 0.069	1
AGES J223506+233707	22:35:05.6	0.7	23:37:07	10	5655 ± 3	139 ± 6	159 ± 8	6.4 ± 0.6	0.754 ± 0.082	0
AGES J223517+244317	22:35:16.8	0.7	24:43:17	11	9954 ± 8	193 ± 15	233 ± 23	3.4 ± 0.6	0.348 ± 0.079	1
AGES J223605+242407	22:36:04.7	0.7	24:24:07	11	16062 ± 5	68 ± 11	104 ± 16	4.0 ± 0.5	0.262 ± 0.055	1
AGES J223613+243504	22:36:13.0	0.7	24:35:04	10	12790 ± 3	265 ± 5	284 ± 8	7.9 ± 0.7	1.179 ± 0.111	0
AGES J223627+234258	22:36:27.2	0.7	23:42:58	10	1410 ± 2	59 ± 4	74 ± 6	9.5 ± 0.7	0.522 ± 0.065	0
AGES J223628+245307	22:36:27.8	2.2	24:53:07	54	12893 ± 10	195 ± 20	242 ± 29	7.2 ± 1.5	0.771 ± 0.202	1
AGES J223631+240823	22:36:30.6	0.7	24:08:23	10	12041 ± 6	68 ± 11	124 ± 17	6.1 ± 0.7	0.366 ± 0.066	0
AGES J223701+225532	22:37:00.8	0.7	22:55:32	10	11519 ± 3	195 ± 7	229 ± 10	6.8 ± 0.6	1.146 ± 0.099	0
AGES J223715+232957	22:37:15.0	0.7	23:29:57	12	18562 ± 9	142 ± 17	188 ± 26	3.3 ± 0.6	0.324 ± 0.078	1
AGES J223739+244947	22:37:39.1	0.7	24:49:47	12	15071 ± 4	276 ± 9	291 ± 13	5.9 ± 0.9	0.944 ± 0.152	0
AGES J223741+242520	22:37:41.0	0.7	24:25:20	10	8782 ± 2	165 ± 4	181 ± 6	8.2 ± 0.6	1.033 ± 0.092	0
AGES J223745+225309	22:37:45.0	0.7	22:53:09	11	11500 ± 5	63 ± 9	94 ± 14	5.2 ± 0.7	0.240 ± 0.056	1
AGES J223746+234712	22:37:46.5	0.7	23:47:12	10	1341 ± 2	325 ± 4	348 ± 5	36.3 ± 2.0	9.1 ± 0.9	3
AGES J223823+245207	22:38:22.7	0.7	24:52:07	11	15323 ± 6	205 ± 12	230 ± 17	8.4 ± 1.5	0.556 ± 0.150	1
AGES J223829+235135	22:38:29.4	0.7	23:51:35	10	1414 ± 3	36 ± 6	73 ± 8	8.3 ± 0.6	0.351 ± 0.047	0
AGES J223834+231114	22:38:34.4	0.7	23:11:14	11	8770 ± 6	154 ± 12	192 ± 18	5.2 ± 0.7	0.691 ± 0.108	0
AGES J223839+234247	22:38:39.0	0.7	23:42:47	11	8797 ± 7	90 ± 14	163 ± 21	5.4 ± 0.7	0.422 ± 0.073	0
AGES J223842+233156	22:38:42.3	0.7	23:31:56	10	11824 ± 4	239 ± 8	265 ± 12	4.7 ± 0.6	0.689 ± 0.085	0
AGES J223846+234923	22:38:45.6	0.8	23:49:23	21	8788 ± 6	153 ± 11	195 ± 17	4.3 ± 0.5	0.436 ± 0.070	0
AGES J223900+244752	22:39:00.1	0.8	24:47:52	11	14965 ± 4	302 ± 8	328 ± 12	6.6 ± 0.8	0.950 ± 0.117	0
AGES J223905+240651	22:39:05.1	0.7	24:06:51	10	8842 ± 6	169 ± 11	248 ± 17	6.2 ± 0.6	1.024 ± 0.096	0
AGES J223946+242157	22:39:46.3	0.7	24:21:57	11	7493 ± 5	44 ± 10	120 ± 16	6.8 ± 0.6	0.350 ± 0.055	0
AGES J224005+244154	22:40:04.6	0.7	24:41:54	10	12805 ± 4	379 ± 8	469 ± 13	16.2 ± 1.1	3.981 ± 0.212	0
AGES J224016+244658	22:40:16.3	0.7	24:46:58	11	15979 ± 7	71 ± 15	120 ± 22	4.8 ± 0.7	0.257 ± 0.069	0
AGES J224024+243019	22:40:24.0	0.7	24:30:19	11	8856 ± 5	43 ± 11	90 ± 16	5.7 ± 0.7	0.222 ± 0.052	0
AGES J224025+243925	22:40:24.9	0.8	24:39:25	12	16026 ± 3	237 ± 6	245 ± 9	4.1 ± 0.6	0.549 ± 0.093	1
AGES J224039+243229	22:40:39.0	0.7	24:32:29	11	12855 ± 4	171 ± 9	189 ± 13	3.5 ± 0.5	0.450 ± 0.076	0
AGES J224052+234635	22:40:52.3	0.8	23:46:35	11	11745 ± 2	85 ± 5	95 ± 7	5.6 ± 0.7	0.336 ± 0.065	0
AGES J224110+243500	22:41:09.9	0.7	24:35:00	10	9047 ± 2	192 ± 5	212 ± 7	12.3 ± 0.9	1.957 ± 0.149	0
AGES J224125+232228	22:41:25.5	0.8	23:22:28	11	7181 ± 5	62 ± 10	181 ± 15	29.0 ± 1.9	1.927 ± 0.201	1

AGES J224005+244154 is a galaxy in the background of the NGC 7332 field with a very large HI mass of  $3.1 \times 10^{10} M_{\odot}$ . It has a 1.4 GHz luminosity of  $6.9 \times 10^{22} \text{ W Hz}^{-1}$  (from the NVSS; Condon et al. 1998) and a far IR (FIR) luminosity of  $8.1 \pm 2.2 \times 10^{10} L_{\odot}$  (from IRAS; Moshir et al. 1990). Neither the NVSS source nor the IR source had previously been associated either with each other or with an optical counterpart.

The ratio of the FIR and 1.4 GHz fluxes gives a  $q$  value of 2.07 (Helou 1985). A  $q$  value of less than 1.64 would indicate that a radio-loud AGN dominated the 1.4 GHz continuum, while higher values indicate that star formation is dominant. The  $q$  value for AGES J224005+244154 thus implies that the source of the 1.4 GHz continuum is star formation rather than an AGN. Using the equations of Yun, Reddy & Condon (2001), the FIR flux indicates a current SFR of  $21 \pm 9 M_{\odot} \text{ yr}^{-1}$  while the 1.4 GHz flux

gives a current SFR of  $41 \pm 12 M_{\odot} \text{ yr}^{-1}$ . These are both consistent with an SFR of  $\sim 30 M_{\odot} \text{ yr}^{-1}$ ; at this rate, the galaxy has a gas-consumption timescale of just 1 Gyr, putting it in the starburst category.

We observed this galaxy with the VLA of NRAO<sup>6</sup> in order to determine firstly whether it was a single source and, if so, whether it showed signs of a recent interaction that might have triggered a star burst. The galaxy was observed in C configuration in April 2008 for a total of 6 hours. The observations were centered at a frequency of 1362.22 MHz (corresponding to  $12805 \text{ km s}^{-1}$ , the AGES velocity of the galaxy) with a bandwidth of 6.25 MHz over 64 spectral channels, resulting in a velocity resolution of  $21.5 \text{ km s}^{-1}$ . The data were reduced using the

<sup>6</sup> The National Radio Astronomy Observatory is a facility of the National Science Foundation operated under cooperative agreement by Associated Universities, Inc.

TABLE 2  
L-BAND FOLLOW-UP OBSERVATIONS

AGES ID	Receiver	Backend	No. Obs.	R.A. (J2000)	Decl.) (J2000)	Velocity (km s <sup>-1</sup> )	Status
J025542+253222	LBW	IC	4	02:55:42.0	25:32:22	14973	Unconfirmed
J025626+254614	LBW	IC	1	02:56:26.0	25:46:14	10385	Confirmed
J025711+254925	LBW	IC	2	02:57:11.0	25:49:25	10430	Unconfirmed
J025720+245431	LBW	IC	1	02:57:19.5	24:54:31	2310	Unconfirmed
J025742+261755	LBW	IC	1	02:57:42.4	26:17:55	10384	Confirmed
J025800+252143	LBW	WAPP	2	02:57:59.7	25:21:43	6924	Unconfirmed
J025801+255804	LBW	IC	2	02:58:00.8	25:58:04	6989	Unconfirmed
J025817+241737	LBW	IC	1	02:58:17.0	24:17:37	10243	Unconfirmed
J025824+251514	LBW	IC	1	02:58:24.2	25:15:14	560	Unconfirmed
J025828+253058	LBW	IC	2	02:58:27.9	25:30:58	6938	Unconfirmed
J025902+253518	LBW	IC	1	02:59:04.0	25:35:10	7120	Confirmed
J025924+243433	LBW	IC	2	02:59:24.0	24:34:33	14050	Unconfirmed
J025936+253446	LBW	WAPP	3	02:59:36.0	25:34:46	10253	Confirmed
J030025+255335	LBW	WAPP	1	03:00:25.0	25:53:35	10611	Confirmed
J030036+241156	LBW	IC	2	03:00:30.0	24:11:32	15180	Confirmed
J030104+243724	LBW	IC	2	03:01:03.5	24:37:24	11109	Unconfirmed
J030107+253206	LBW	IC	1	03:01:07.4	25:32:06	436	Unconfirmed
J030114+260059	LBW	IC	1	03:01:13.9	26:00:59	14050	Unconfirmed
J030116+245206	LBW	IC	1	03:01:16.3	24:52:06	11086	Unconfirmed
J030214+250805	LBW	IC	1	03:02:13.8	25:08:05	458	Unconfirmed
J030313+245749	LBW	IC	2	03:03:13.0	24:57:49	9790	Unconfirmed
J030428+244322	LBW	IC	1	03:04:28.0	24:43:22	15968	Unconfirmed
J030450+260045	LBW	IC	1	03:04:50.0	26:00:45	9420	Confirmed
J030506+244308	LBW	IC	1	03:05:06.0	24:43:08	14450	Unconfirmed
J030528+242441	LBW	IC	2	03:05:28.0	24:24:41	15000	Unconfirmed
J223111+234146	LBW	WAPP	2	22:31:11.0	23:41:46	16645	Confirmed
J223143+244513	LBW	WAPP	1	22:31:42.9	24:45:11	16130	Confirmed
J223226+231111	ALFA+LBW	WAPP	2+1	22:32:26.1	23:11:11	18256	Unconfirmed
J223231+231601	LBW	WAPP	1	22:32:31.3	23:16:11	11797	Confirmed
J223237+231209	ALFA	WAPP	3	22:32:37.0	23:12:05	16619	Confirmed
J223240+224548	ALFA	WAPP	1	22:32:40.6	22:45:48	11481	Unconfirmed
J223314+241428	LBW	WAPP	1	22:33:14.8	24:14:28	7463	Unconfirmed
J223318+244545	LBW	WAPP	1	22:33:17.5	24:45:38	12233	Confirmed
J223355+243114	ALFA	WAPP	1	22:33:54.8	24:31:17	10011	Confirmed
J223404+240213	ALFA	WAPP	1	22:34:04.1	24:02:13	16121	Unconfirmed
J223415+233057	LBW	WAPP	2	22:34:15.8	23:30:59	16487	Confirmed
J223502+235258	ALFA+LBW	WAPP	1+1	22:35:02.5	23:52:33	9637	Confirmed
J223502+242142	ALFA	WAPP	1	22:35:02.7	24:21:42	12242	Confirmed
J223517+244317	ALFA	WAPP	1	22:35:16.7	24:43:15	9956	Confirmed
J223544+235401	ALFA	WAPP	1	22:35:44.0	23:54:01	16471	Unconfirmed
J223605+242407	LBW	WAPP	1	22:36:04.6	24:24:06	16067	Confirmed
J223628+245307	LBW	WAPP	1	22:36:27.7	24:53:07	12893	Confirmed
J223715+232957	LBW	WAPP	2	22:37:14.6	23:30:04	18560	Confirmed
J223745+225309	LBW	WAPP	1	22:37:45.2	22:53:04	11499	Confirmed
J223823+245207	LBW	WAPP	1	22:28:23.9	24:52:08	15259	Confirmed
J223957+233942	ALFA	WAPP	1	22:39:57.0	23:39:42	16574	Unconfirmed
J224025+243925	ALFA+LBW	WAPP	1+2	22:40:25.0	24:39:27	16026	Confirmed
J224125+232228	LBW	WAPP	1	22:41:25.4	23:22:26	7181	Confirmed

TABLE 3  
OPTICAL REDSHIFTS

AGES ID	Optical Velocity (km s <sup>-1</sup> )	H I Velocity (km s <sup>-1</sup> )
J025737+244321	10437 ± 82	10452 ± 11
J025753+255737	10422 ± 82	10421 ± 3
J025835+241844	10170 ± 133	10147 ± 5
J030008+241600	15090 ± 64	15081 ± 5
J030112+242411	9892 ± 142	9781 ± 4
J030136+245602	10372 ± 74	10417 ± 8
J030146+254314	11238 ± 64	11216 ± 3
J030325+241510	14786 ± 76	14750 ± 8
J223213+232657	16916 ± 119	16892 ± 3
J223449+240744	16298 ± 81	16289 ± 2
J223613+243504	12742 ± 69	12790 ± 3
J223627+234258	1440 ± 88	1410 ± 2
J224005+244154	12799 ± 100	12805 ± 4
J224110+243500	9030 ± 94	9047 ± 2



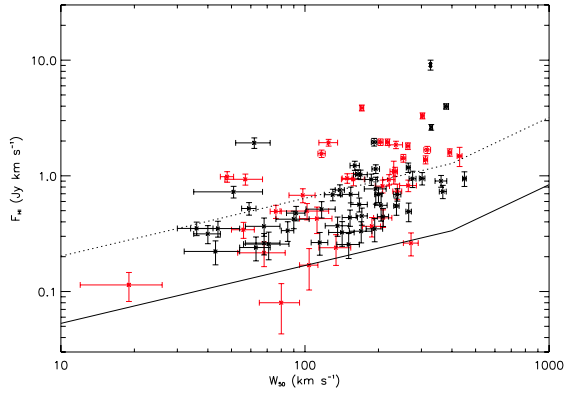


FIG. 3.— Velocity width at 50 per cent of the peak flux versus the integrated flux. The solid line shows the  $\text{SNR} = 5$  (approximate) detection limit, and the dotted line shows the ALFALFA ‘solid detection’ limit (Kent et al. 2009). Black symbols represent sources from the NGC 7332 region and red symbols sources from the NGC 1156 region.

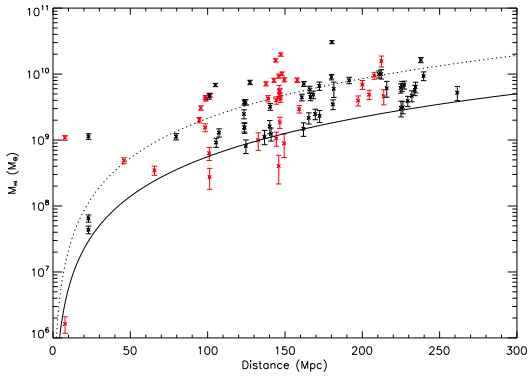


FIG. 4.— HI mass versus distance. The solid line shows the  $\text{SNR} = 5$  (approximate) detection limit and the dotted line shows the ALFALFA ‘solid detection’ limit (all for  $W_{50} = 200 \text{ km s}^{-1}$ ). Red symbols indicate sources from the NGC 1156 region and black symbols sources from the NGC 7332 region.

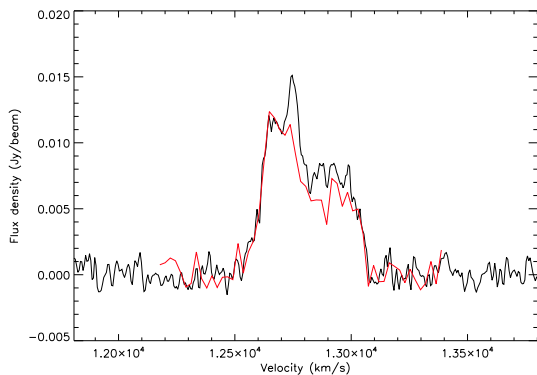


FIG. 5.— Arecibo spectrum of AGES J224005+244154 (black) with the VLA spectrum overlaid (red).

Astronomical Image Processing System (AIPS).

The VLA data reached a noise level of  $\sim 0.3 \text{ mJy}$ . Cleaning was carried out to a depth of  $1 \text{ mJy}$ , and a moment 0 map was made using a  $1 \text{ mJy}$  clipping. This map was used to mask the part of the image containing signal from the galaxy. The flux recovered from this region with the VLA was  $3.49 \pm 0.09 \text{ Jy km s}^{-1}$ , compared to

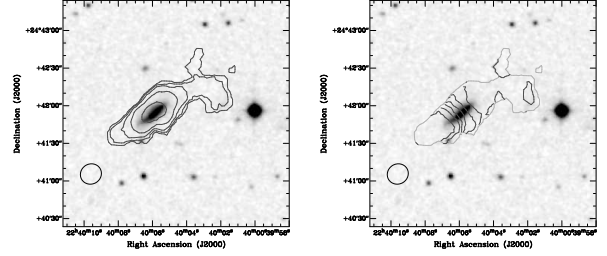


FIG. 6.— Moment 0 (left) and 1 (right) maps of AGES J224005+244154 overlaid on a DSS  $B$ -band image. The contour levels for the moment 0 map are 40, 80, 160, 320 and  $640 \text{ Jy beam}^{-1} \text{ km s}^{-1}$ . The contour levels for the moment 1 map are  $12600$  to  $12850 \text{ km s}^{-1}$  in steps of  $50 \text{ km s}^{-1}$ , with the higher velocities to the east (left) of the image.

$3.98 \pm 0.21 \text{ Jy km s}^{-1}$  with Arecibo, a difference of less than  $2.5 \sigma$ . The spectrum from this region of the VLA data appears consistent with the Arecibo spectrum (Fig. 5). It thus appears that little extended or lower-level flux has been missed with the VLA.

As can be seen from Figure 6, the galaxy is disturbed in both the HI and the optical. The optical disturbance can be seen as a faint plume at the eastern end of the galaxy; the HI disturbance is much more visible and takes the form of a large plume at the western end of the galaxy. The velocity field is fairly smooth over the main disc of the galaxy, but is again disturbed at the western end.

AGES J224005+244154 is clearly not evolving in isolation. It seems most likely that it has recently undergone a merger with a smaller galaxy that has triggered the current starburst phase and has resulted in the disturbances seen in the optical and HI images.

#### 4.5. $H\alpha$ observations of AGES J030039+254656

AGES J030039+254656 is a new dwarf galaxy discovered by AGES in the neighborhood of NGC 1156. CCD images in the  $H\alpha$ -line and continuum were obtained during an observing run in November 2007 under seeing of  $1.8''$ . The observations were performed by Serafim Kaisin with the BTA 6-m telescope of the Special Astrophysical Observatory equipped with the SCORPIO focal reducer. A CCD chip of  $2048 \times 2048$  pixels provides a total field of view of about  $6.1'$  with a scale of  $0.18''/\text{pixel}$ . The images in  $H\alpha + [\text{NII}]$  and continuum were obtained via observing the galaxy through a narrow-band interference filter  $H\alpha$  ( $\Delta\lambda = 75 \text{ \AA}$ ) with an effective wavelength  $\lambda = 6555 \text{ \AA}$  and two medium-band filters for the continuous spectrum SED607 with  $\Delta\lambda = 167 \text{ \AA}$ ,  $\lambda = 6063 \text{ \AA}$  and SED707 with  $\Delta\lambda = 207 \text{ \AA}$ ,  $\lambda = 7063 \text{ \AA}$ , respectively. Exposure times for the galaxy were  $2 \times 300 \text{ s}$  in the continuum and  $2 \times 600 \text{ s}$  in  $H\alpha$ .

Our data reduction followed the standard practice and was performed within the MIDAS package. For all the data bias was subtracted and the images were flat-fielded by twilight flats. Cosmic particles were removed and the sky background was subtracted. Then the images in the continuum were normalized to  $H\alpha$  images using 5–15 field stars and subtracted.  $H\alpha$  fluxes were obtained for the continuum-subtracted images, using spectrophotometric standard stars observed in the same nights as the object. The continuum-subtracted and  $R$ -band continuum images are shown in Figure 7. The investigation of measurement errors contributed from the continuum

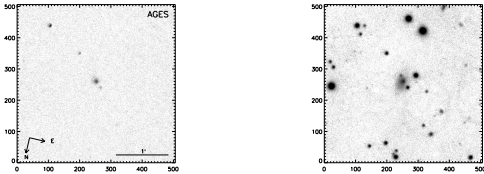


FIG. 7.— Continuum-subtracted AGES  $H\alpha$  (left) and  $R$ -band continuum (right) images of AGES J030039+254656. The orientation and scale are given in the left panel and are the same for both images.

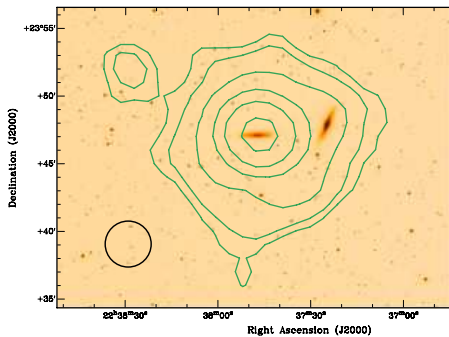


FIG. 8.— Integrated H I (moment 0) map of the NGC 7332 group overlaid on the digitized sky survey image of the region. Contours are at 3, 5, 10, 25, 50 and 100  $\sigma$ , where  $1\sigma = 0.04 \text{ Jy km s}^{-1} \text{ beam}^{-1} = 1.5 \times 10^{18} \text{ cm}^{-2}$ . The AGES beam is shown as a black ellipse at the bottom-left.

subtraction, flat-fielding and scatter in the zeropoints has shown that they have typical values within 10%. We did not correct  $H\alpha$  fluxes for the contribution of the [NII] lines, because it is likely to be small for the low-luminosity galaxy. We find an  $H\alpha$  flux of  $7.1 \pm 0.7 \times 10^{-22} \text{ W cm}^{-2}$ , which (after correction for galactic absorption) gives a star formation rate of  $8.7 \pm 0.9 \times 10^{-4} M_{\odot} \text{ yr}^{-1}$ .

## 5. RESULTS AND DISCUSSION

### 5.1. The NGC 7332 group

Three galaxies were detected in neutral hydrogen within the NGC 7332 group. In addition to NGC 7339, two new sources, AGES J223829+235135 and AGES J223627+234258, were found in H I. Both of these have optical counterparts in the Digitized Sky Survey but have not been previously catalogued.

Figure 8 shows the integrated H I (moment 0) map of the group over the velocity range  $1160 - 1520 \text{ km s}^{-1}$ , overlaid on the digitized sky survey image of the region. The two new sources can be seen, and it is also clear that the H I detected at the position of NGC 7332 is associated with NGC 7339.

No obvious tidal streams or H I clouds were found in the group. For a velocity width of  $50 \text{ km s}^{-1}$ , the  $5\sigma$  detection limit would be a column density of  $4 \times 10^{18} \text{ cm}^{-2}$  for features that fill the beam (FWHM = 23 kpc at the distance of NGC 7332). The limit for features that do not fill the beam will rise as the reciprocal of their filling factor; a feature with a column density of  $10^{20} \text{ cm}^{-2}$  would be seen down to a filling factor of 4 per cent, for instance.

#### 5.1.1. NGC 7332 and NGC 7339

The flux of NGC 7339 was found by fitting a 2D Gaussian as described in Section 2.1. This gave a beam-

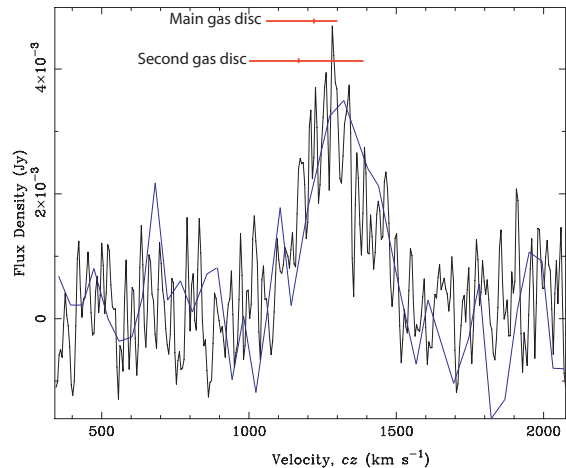


FIG. 9.— H I spectrum at the position of NGC 7332. This matches very well with the detection of Knapp et al. (1978), which is overlaid in blue. The two red bars at the top indicate the central velocity (vertical tick) and the velocity extent (horizontal length) of the main and second (counter-rotating) ionised gas discs seen in NGC 7339 by Plana & Boulesteix (1996). It can be seen that the neutral hydrogen is at a generally higher velocity than the ionised gas, although there is a significant overlap.

corrected flux of  $9.1 \pm 0.9 \text{ Jy km s}^{-1}$  and deconvolved major and minor axes (FWHM of the Gaussian) for the H I of  $215 \pm 14 \times 167 \pm 11$  arc seconds, at a position angle of  $81 \pm 9$  degrees (north through east). The fitted position for the H I is  $22:37:46.2, 23:47:12, 0.2$  arc minutes from the position in NED (taken from the 2MASS catalog, Jarrett et al. 2000). The position angle is consistent with alignment of the neutral hydrogen with the optical disc of the galaxy.

Our results are consistent with the flux measured using the Lovell Telescope at Jodrell Bank by Staveley-Smith & Davies (1987) of  $9.8 \pm 1.5 \text{ Jy km s}^{-1}$ . From our determination of the size of the H I, the galaxy should appear as a point source to the Lovell Telescope (beam size  $\sim 12$  arc minutes), so the Staveley-Smith & Davies flux should not be affected by the size of the source.

We find flux at the position of NGC 7332 (Fig. 9) which matches very well with the detection of Knapp et al. (1978). As the ALFA receiver has much lower sidelobes than the old circular feed used by Knapp et al., such a match would not be expected if their detection were merely NGC 7339 in the sidelobes, as has been suggested (Biermann, Clarke & Fricke 1979; Haynes 1981). Our mapping of the region (Figs. 8 and 10) shows that the gas disc of NGC 7339 is distorted, presumably by an interaction with NGC 7332. The gas at this position appears to be part of this distorted disc rather than a separate peak in the H I distribution associated with NGC 7332.

Morganti et al. (2006) detected a small gas cloud between NGC 7332 and NGC 7339 with the WSRT (FWHM  $46'' \times 31''$ ). This is too small and distant to account for the neutral hydrogen we see at the position of NGC 7332. It seems likely that we are seeing lower column-density gas not seen by the WSRT that is at or

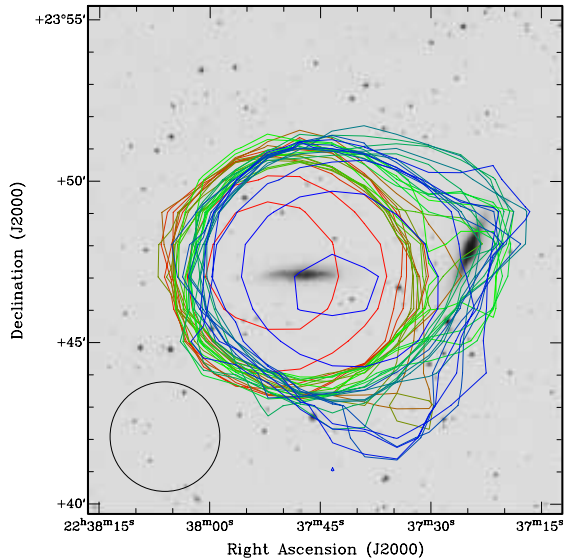


FIG. 10.— Renzogram of the H I in NGC 7339 overlaid on the Digitized Sky Survey *B*-band image of the region showing NGC 7332 (right) and NGC 7339 (centre). This shows contours at the  $5\sigma$  ( $2 \text{ mJy beam}^{-1}$ ) level, colour-coded to indicate the velocity channel from which there were taken (blue for lower recessional velocity, red for higher). The rotation of NGC 7339 can be clearly seen, with the west side having a lower recessional velocity and the east higher. The majority of the distortion over the position of NGC 7332 occurs at intermediate velocities ( $\sim 1300 \text{ km s}^{-1}$ ), indicated by green contours. The black ellipse at the lower left shows the size of the Arecibo beam.

near the position of NGC 7332 – our observations are  $\sim 4$  times more sensitive to low column-density gas that fills the beam (albeit with a larger beam). It is possible that the Morganti et al. cloud is part of a low column-density stream that is feeding the counter-rotating disc in NGC 7332.

### 5.1.2. Dwarf galaxies in the NGC 7332 group

The two new H I sources reported here (AGES J223627+234258 and AGES J223829+235135) both lie in the same velocity range as NGC 7339, at around  $1400 \text{ km s}^{-1}$  and outside the area mapped by Haynes (1981). The spectra and optical (SDSS) images of these galaxies are shown in Figure 11. Both of the new galaxies appear to be narrow, single-peaked sources, which is consistent with their being dwarf galaxies. No tidal features can be definitively identified linking them to the NGC 7332/9 pair, but that these could be present at even lower column-densities than we reach here cannot be ruled out.

The data cube was examined at the positions of the candidate dSph galaxy identified in our optical survey of the region (see §4.2) and also at the positions of the candidate dSph galaxies KKR 73 and KKR 72 identified by Karachentseva et al. (1999). This search found no neutral hydrogen signals in the redshift range of the group.

Our observations can place a limit on the H I mass of these three undetected galaxies (assuming them to be in the group) of  $1.4 \times 10^7 M_{\odot}$ , almost an order of magnitude lower than the Huchtmeier et al. (2000) observations. However, if these are dSph galaxies, as appears to be the case from their optical morphologies, then their non-detection at this limit is not surprising and we can neither confirm nor rule out their being members of the group.

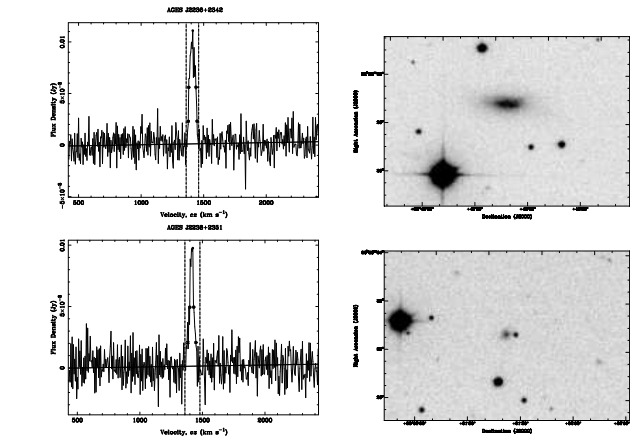


FIG. 11.— H I spectra (left) and Sloan Digital Sky Survey *g*-band images (right) of AGES J223627+234258 (top) and AGES J223829+235134 (bottom).

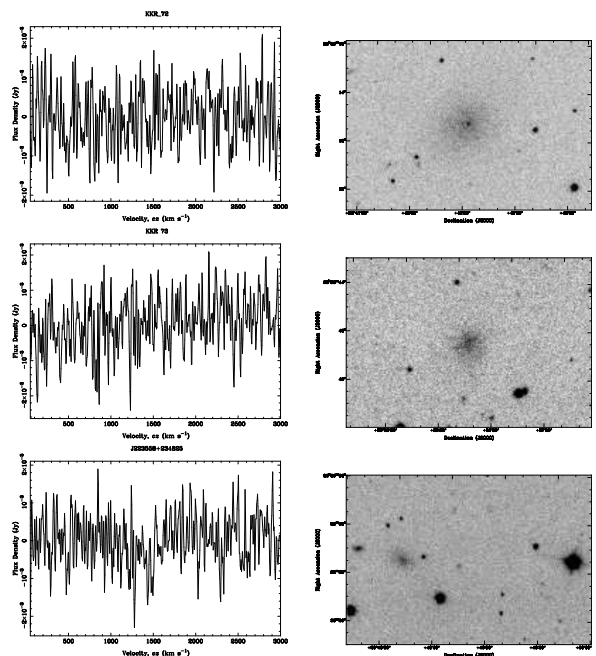


FIG. 12.— Left: H I spectra at the positions of the dwarf spheroidal candidates KKR 72 (top), KKR 73 (center) and J223558+234825 (bottom). These show no detection in the range  $50 - 3000 \text{ km s}^{-1}$ . Right: Sloan Digital Sky Survey *g* band images of the galaxies. Note that J223558+234825 is on the left of the image, due to its proximity to a scan boundary.

The spectra and DSS images are shown in Fig. 12.

Our H I mapping and optical search have brought the total number of possible dwarf galaxies in the group to five, two of which are gas-rich and are confirmed as group members. This gives an overall ratio of small to large galaxies of  $1 - 2.5$  and of small to large H I-rich galaxies of  $2$ . The group appears, therefore, to be less dwarf-rich than would be expected from the HIPASS H I mass function (Zwaan et al. 2005), which (for our limit of  $1.4 \times 10^7 M_{\odot}$ ) predicts  $5.0_{-1.2}^{+1.5}$  galaxies less than  $10^8 M_{\odot}$  for each galaxy above  $10^9 M_{\odot}$ . However, this under-density is less than a  $2\sigma$  result and thus may simply be due to random fluctuations.

### 5.1.3. Properties of the group galaxies

All of the members and potential members of the NGC 7332 group have been covered by the SDSS. We have carried out ellipse fitting on the SDSS  $g$ -band data using the Starlink ESP package in order to find the surface-brightness profiles of the dwarf galaxies (including those from Karachentseva et al. 1999) and have made exponential fits to these profiles. These fits were extrapolated to find the total luminosity of the galaxy.  $g - r$  colours were found using apertures fitted to cover as much of the galaxy as possible without including other sources. One galaxy (KKR 72) had a significant inner component on the surface-brightness profile, this was fitted with a second exponential after subtraction of the fit to the outer regions and was found to contribute negligibly to the overall luminosity.

The results of our fitting are shown in Table 4. Column (1) gives the ID of the galaxy. Columns (2) and (3) give the optical R.A. and declination, as found from the SDSS. Columns (4) and (5) give the central surface-brightness and the scale length for the exponential fit. Column (6) gives the extrapolated total  $g$ -band magnitude. Column (7) gives the  $g - r$  colour and Column (8) gives the  $g$ -band absolute luminosity, corrected for a  $g$ -band extinction of 0.15 mag. (from the IRSA extinction calculator).

We find that AGES J223627+234258 has a fairly low HI mass to light ratio for a dwarf irregular of  $0.13 \pm 0.01 M_{\odot}/L_{\odot}$ . AGES J223829+235135 is more interesting, with a high HI mass to light ratio of  $2.0 \pm 0.2 M_{\odot}/L_{\odot}$ , a very blue colour ( $g - r = 0.1 \pm 0.1$ ), and a fairly low surface brightness (although not as low as the dSph candidates). From both its optical appearance and its high gas fraction, this would appear to be an under-evolved dIrr galaxy, possibly similar to those studied in the Cen A group by Grossi et al. (2007).

The neutral hydrogen properties of the known or suspected members of the NGC 7332 group are given in Table 5. Column (1) gives the ID of the galaxy. Column (2) gives the velocity. This is the HI velocity measured from our datacube where the source is detected and the optical velocity from Simien & Prugniel (1997) for NGC 7332. Column (3) gives the velocity width at 50% of the peak flux. For the detections, this is measured from our datacube, otherwise it is the velocity width assumed in producing the flux limit (shown in italics). Column (4) gives the integrated flux, with an upper limit (based on a  $3-\sigma$  limit of 2.25 mJy multiplied by the assumed velocity width) for non-detections and Column (5) gives this translated into a mass (or mass limit) at the adopted distance of 23 Mpc for the group. Column (6) gives the HI mass to light ratio derived from the measured HI mass and the SDSS  $g$ -band luminosity. For NGC 7332 and NGC 7339, the  $g$ -band luminosity has been calculated using the  $B_T$  and  $V_T$  magnitudes from the RC3 (de Vaucouleurs et al. 1991) and the transformation  $g = V + 0.60(B - V) - 0.12 \pm 0.02$  from the SDSS web pages, giving  $g = 11.5 \pm 0.3$  for NGC 7332 and  $g = 12.7 \pm 0.3$  for NGC 7339.

### 5.2. NGC 1156 and the surrounding region.

NGC 1156 was analysed in the same manner as NGC 7339 (above). This gave a beam-corrected integrated flux of  $75.6 \pm 6.4 \text{ Jy km s}^{-1}$ , which is consistent with the values of Swaters et al. (2002) and Haynes et al. (1998). This

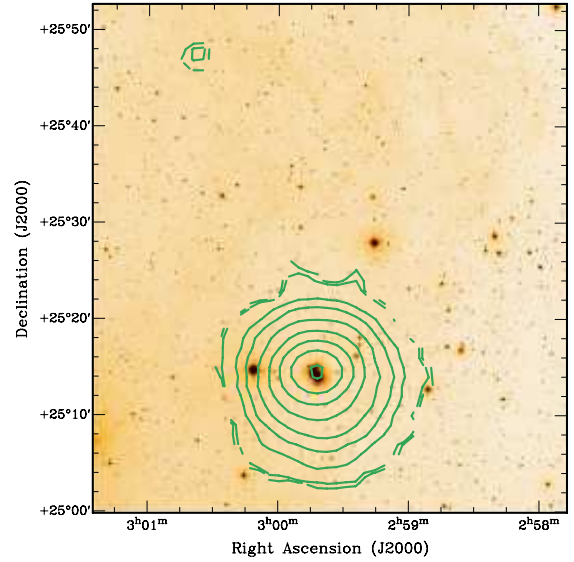


FIG. 13.— DSS2  $B$ -band image of the NGC 1156 region overlaid with contours from a 3-sigma clipped integrated HI (moment 0) map. Contours are at 0.05, 0.1, 0.2, 0.5, 1, 2, 4, 8, 16 and 32  $\text{Jy km s}^{-1}$ .

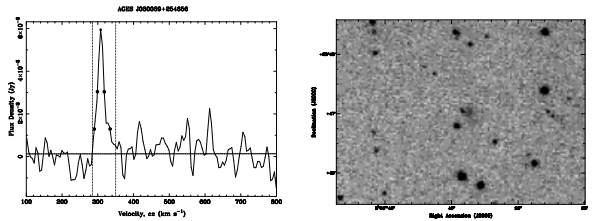


FIG. 14.— HI spectrum (left) and Super-COSMOS scanned POSS II  $B_J$ -band image (right) of AGES J030039+254656.

gives an HI mass for the galaxy of  $1.08 \pm 0.09 \times 10^9 M_{\odot}$ . The fitted gaussian has deconvolved major and minor axes of  $272 \pm 16$  and  $212 \pm 13$  arc seconds respectively, at a position angle of  $93 \pm 3$  degrees (north through east), which appears consistent with the Swaters et al. WSRT map of the galaxy. The fitted position of the galaxy is  $02:59:52.3, 25:14:30$  (J2000), 0.3 arc minutes from the NED position (taken from the 2MASS catalog, Jarrett et al. 2000).

AGES J030039+254656 is a small dwarf galaxy found 35 arc minutes north-north-east of NGC 1156 (80 kpc in projection), as can be seen in Figure 13 showing the integrated HI (moment 0) map. An optical counterpart is clearly visible on the digitized sky survey (see Figure 14) at  $03:00:38.6, 25:47:02$  (J2000). It has an HI flux of  $0.114 \pm 0.032 \text{ Jy km s}^{-1}$ , giving it a neutral hydrogen mass of  $1.63 \pm 0.46 \times 10^6 M_{\odot}$ .

As stated in §4.5, we measure a SFR of  $8.7 \pm 0.9 \times 10^{-4} M_{\odot} \text{ yr}^{-1}$  for AGES J030039+254656, compared to  $0.71 \pm 0.07 M_{\odot} \text{ yr}^{-1}$  for NGC 1156. The star-formation rate and HI mass are thus both around three order of magnitudes lower than NGC 1156. From the Super-COSMOS plate-scanning survey (see §5.3), we find  $B_J = 20.14 \pm 0.3$ ,  $R = 19.69 \pm 0.3$  and  $B - R = 0.45 \pm 0.07$ . Using the extinction maps of Schlegel et al. (1998), we find a very blue corrected color of  $B - R = -0.03$  and  $L_B = 2.7 \pm 0.8 \times 10^6 L_{\odot}$ , giving  $M_{HI}/L_B = 0.61 \pm 0.26 M_{\odot}/L_{\odot}$ .

The new galaxy is on the same side of the galaxy as the possible tidal tail reported by Hunter et al. (2002) as

TABLE 4  
SDSS PROPERTIES OF THE DWARF GALAXIES IN THE NGC 7332 GROUP.

ID	RA	Dec.	$\mu_0(g)$	$h_g$	$m_g$	$g - r$	$L_g$
(1)	(J2000) (2)	(J2000) (3)	(mag arcsec <sup>-2</sup> ) (4)	(arcsec) (5)	(mag) (6)	(mag) (7)	( $10^7 L_\odot$ ) (8)
KKR 73	22:35:40.60	23:36:26.6	$23.51 \pm 0.02$	$6.3 \pm 0.2$	$17.5 \pm 0.2$	$0.5 \pm 0.1$	$6.7 \pm 0.5$
J223558+234825	22:35:58.04	23:48:22.4	$23.51 \pm 0.02$	$4.40 \pm 0.15$	$18.3 \pm 0.2$	$0.5 \pm 0.1$	$3.2 \pm 0.2$
KKR 72	22:36:11.75	23:42:43.46	$23.59 \pm 0.02$	$12.4 \pm 0.2$	$16.1 \pm 0.1$	$0.4 \pm 0.1$	$24.1 \pm 1.6$
AGES J223627+234258	22:36:27.82	23:42:59.4	$21.84 \pm 0.06$	$7.98 \pm 0.16$	$15.3 \pm 0.1$	$0.4 \pm 0.1$	$49.8 \pm 1.9$
AGES J223829+235135	22:38:29.69	23:51:31.1	$22.28 \pm 0.02$	$2.26 \pm 0.05$	$18.5 \pm 0.1$	$0.1 \pm 0.1$	$2.6 \pm 0.1$

TABLE 5  
HI PROPERTIES OF THE NGC 7332 GROUP GALAXIES.

ID	Vel.	$\Delta V_{50}$	$F_{HI}$	$M_{HI}$	$M_{HI}/L_g$
(1)	(km s <sup>-1</sup> ) (2)	(km s <sup>-1</sup> ) (3)	(Jy km s <sup>-1</sup> ) (4)	( $10^7 M_\odot$ ) (5)	( $M_\odot/L_\odot$ ) (6)
KKR 73	...	$50^a$	$< 0.11$	$< 1.4$	$< 0.21$
J223558+234825	...	$50^a$	$< 0.11$	$< 1.4$	$< 0.44$
KKR 72	...	$50^a$	$< 0.11$	$< 1.4$	$< 0.06$
AGES J223627+234258	1409	58	$0.54 \pm 0.02$	$6.7 \pm 0.3$	$0.13 \pm 0.01$
NGC 7332	1172	$300^a$	$< 0.68$	$< 8.4$	$< 0.005$
NGC 7339	1341	327	$9.1 \pm 0.9$	$114 \pm 11$	$0.19 \pm 0.03$
AGES J223829+235135	1414	32	$0.41 \pm 0.3$	$5.1 \pm 0.4$	$2.0 \pm 0.2$

<sup>a</sup> Value used in estimating upper limits

having been seen in VLA observations. This possible tail stretched 3' south-east from an HI complex to the north-east of the galaxy that has an unusually large velocity spread. The tail is not seen in the AGES data, however as its length is less than the Arecibo beam size we would not expect to be able to distinguish it from the main body of HI in NGC 1156.

Following Verley et al. (2007), we can estimate the ratio of the tidal force being exerted currently by AGES J030039+254656 to the binding force of NGC 1156. If we assume that the HI mass can be related to the total mass by  $M_{\text{tot}} = \gamma M_{\text{HI}}$  and use the HI radius of 212 arcseconds measured for NGC 1156 by Swaters et al. (2002), then:

$$Q_{ip} = \frac{F_{\text{tidal}}}{F_{\text{bind}}} = \left( \frac{M_i}{M_p} \right) \left( \frac{D_p}{S_{ip}} \right)^3 \quad (2)$$

Where  $M_i = \gamma_i M_{\text{HI},i}$  is the mass of the interactor (AGES J030039+254646),  $M_p = \gamma_p M_{\text{HI},p}$  is the mass of the primary (NGC 1156),  $D_p$  is the diameter of the primary, and  $S_{ip}$  is the separation between the two galaxies.

This gives  $Q_{ip} = 1.2 \times 10^{-5} \frac{\gamma_i}{\gamma_p}$ , where a value of  $\sim 10^{-2}$  or greater indicates significant tidal forces. The ratio  $\frac{\gamma_i}{\gamma_p}$  would therefore have to be of order a thousand for this to be significant, that is AGES J030039+254656 would have to have a ratio of total mass to HI mass a thousand times higher than that of NGC 1156. It seems unlikely, therefore, that AGES J030039+254656, in its current position, could be exerting any significant tidal force on NGC 1156. However, the possibility of a past interaction cannot be ruled out.

From the radio velocity difference ( $77 \pm 4$  km s<sup>-1</sup>) and the projected separation of 80 kpc between NGC 1156 and AGES J030039+254656, the minimum dynamical

mass of the pair is calculated to be  $1.1 \pm 0.1 \times 10^{11} M_\odot$ , giving  $M_{\text{dyn}}/L_B \geq 65 M_\odot/L_\odot$ .

Having only one (known) dwarf companion, NGC 1156 appears to be well below the average. Between our limit of  $1.4 \times 10^6 M_\odot$  and  $10^8 M_\odot$ , the HIPASS HI mass function (Zwaan et al. 2005) predicts  $17.9_{-5.5}^{+8.1}$  dwarf galaxies for each galaxy of over  $10^9 M_\odot$ ,  $3\sigma$  above what we observe in NGC 1156.

### 5.3. The AGES Volume

The AGES cubes are bandpass-limited at a redshift of around 20,000 km s<sup>-1</sup> and have a combined area of 10 deg<sup>2</sup>. This gives a comoving volume behind NGC 1156 and NGC 7332 of 24,000 Mpc<sup>3</sup>. In this volume we find a further 82 confirmed sources: 46 in the NGC 7332 cube and 36 in the NGC 1156 cube. All the sources have been associated with optical counterparts (see Table 6). Radio sources were correlated both with the APM<sup>7</sup> online sky catalogue and with the SuperCOSMOS<sup>8</sup> sky surveys, yielding identifications within 85 arcseconds in all cases. Table 6 gives the positions of the optical counterparts, the offsets from the HI positions (HI-optical), the  $B_J$  and  $R$  magnitudes from the SuperCOSMOS survey (with errors of 0.3 mag for  $m > 15$ ; Hambly, Irwin & MacGillivray (2001), the HI to  $B_J$  luminosity ratio, the literature name (if any), and the radial velocity (where available) from the NED database<sup>9</sup> (sources for quoted velocities are given in Table 7). For some galaxies in the NGC 1156 region, photometry is available from CFHT observations in  $g$  and  $r$ -bands with the MEGACAM imager. Aperture photometry for these sources is given in footnotes to the table. It should be noted

<sup>7</sup> see <http://www.ast.cam.ac.uk/~{japmcat/>

<sup>8</sup> see <http://www-wfau.roe.ac.uk/sss/pixel.html>

<sup>9</sup> see <http://nedwww.ipac.caltech.edu>

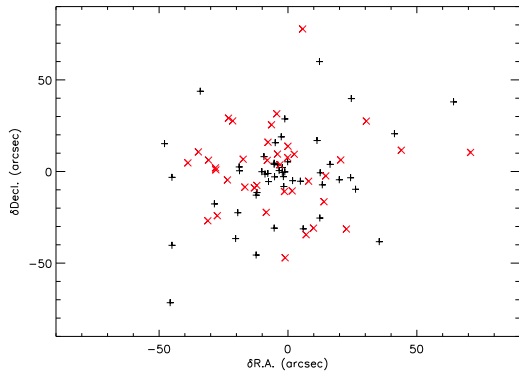


FIG. 15.— Offsets (H I-optical) for sources in the NGC 1156 field (red) and in the NGC 7332 field (black). 90% of the sources have offsets smaller than 51 arcseconds.

that for low surface-brightness galaxies, the SuperCOSMOS magnitudes may dramatically underestimate the luminosity (c.f. Disney & Phillipps 1983); an example of this can be seen with AGES J030014+255335, which has  $M_{HI}/L_B = 11.1 \pm 3.8 M_{\odot}/L_{\odot}$  from the SuperCOSMOS photometry, while the deeper CFHT imaging gives a much more feasible  $M_{HI}/L_g = 2.0 \pm 0.3 M_{\odot}/L_{\odot}$ .

The distribution of separations can be seen in Fig. 15. The median offset between the H I source and the identified optical counterpart is 20 arcsec, with 90 per cent of counterparts falling within 51 arcsec of the H I source. It can be seen that the NGC 1156 field appears to have a less centrally condensed distribution of offsets than the NGC 7332 field, this is borne out by the statistics with the median offset being 26 arcsec in NGC 1156 and only 19 arcsec in NGC 7332. This may be simply natural variation, but could also be due to the strong and variable optical absorption ( $A_B = 0.89$  to 1.45 mags) in the NGC 1156 region which makes identification of optical counterparts difficult. Low surface-brightness counterparts could have been missed, or areas of high absorption on spatial scales smaller than that mapped by Schlegel et al. (1998) could have led to the correct counterpart being dismissed as being too faint.

Examining the correspondance between the errors on the H I positions (Table 1 and the the offsets between the optical and H I positions, it appears that 40/87 of the optical counterparts lie within the R.A. error and 47/87 within the declination error. Treating the RA and dec errors as defining an error ellipse rather than as independent, only 22/87 sources fall within the error ellipse. In order to enclose 69 per cent of the sources (e.g. 1 sigma), the error radius needs to be increased by a factor of 2.95 – it thus appears that the error on the H I position underestimates the true positional uncertainty by around a factor of three.

### 5.3.1. Large Scale Structure

The large velocity range covered by AGES allows us to look at the large scale structure behind the targetted regions. Pie slices (Fig. 16 for NGC 7332 and Fig. 17 for NGC 1156) show the distribution of galaxies in declination and right ascension. These figures also show the previously known galaxies with redshifts, given in Table 7

From Fig. 16, two structures appear to be present be-

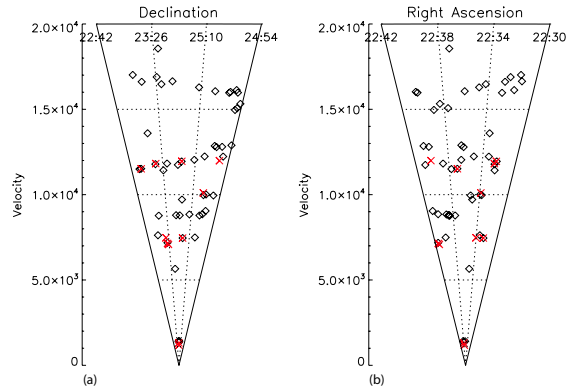


FIG. 16.— Pie-slices of the large scale structure in the region behind NGC 7332: (a) Declination; (b) Right Ascension. Literature galaxies (with redshifts) are shown as red crosses; AGES galaxies are shown as black diamonds. The horizontal axis has been expanded for clarity.

hind NGC 7332. The first, between 11000 and 12500  $\text{km s}^{-1}$  can be seen most easily in the declination slice. The second, between 14000 and 18000  $\text{km s}^{-1}$ , can be seen in both slices. Fitting surfaces to the distribution of galaxies confirms that all 10 galaxies in the lower redshift range and 12 out of 14 in the higher redshift range fall within 300  $\text{km s}^{-1}$  of the fitted surface. The two in the higher redshift range that do not seem to be in the structure both have  $\text{R.A.} > 22^{\text{h}}40^{\text{m}}$ , while the other twelve are all at lower R.A.s.

The redshift range 2000 – 7000  $\text{km s}^{-1}$  behind NGC 7332 is identified by Fairall (1990) as being through void regions. This region does appear to have a lower than normal galaxy density, with only one source (AGES J223506+233707) found. AGES J223506+233707 is a nearly edge-on spiral at a recessional velocity of 5655  $\text{km s}^{-1}$ , giving a distance of 80 Mpc for  $H_0 = 71 \text{ km s}^{-1} \text{ Mpc}^{-1}$ . It does not seem disturbed either in its H I profile or in its optical (SDSS) appearance and has an H I mass of  $1.1 \pm 0.1 \times 10^9 M_{\odot}$ , similar to NGC 1156 and the Large Magellanic Cloud. From aperture photometry performed on SDSS images, it has a  $g = 18.7 \pm 0.4$ , giving  $M_g = -15.8 \pm 0.2$  and  $L_g = 2.3 \times 10^8 L_{\odot}$ . This gives it a high  $M_{HI}/L_g = 4.8 M_{\odot}/L_{\odot}$ . The color (again from aperture photometry on SDSS images) is  $g - r = 0.2 \pm 0.6$ , making this a rather blue galaxy – which is consistent with its high H I mass to light ratio and makes this appear to be an under-evolved galaxy. This may be a good example of a galaxy that has evolved in a void region without interacting significantly with other galaxies and thus has not evolved as fast as other galaxies, but determining whether this is the case would require much future study.

Figure 17 shows large scale structure in the NGC 1156 region, which is clearly present at  $\sim 7000 \text{ km s}^{-1}$  and just about 10 000  $\text{km s}^{-1}$ . However, unlike NGC 7332, these are both visible in literature redshift data, with galaxies around UGC 2445 making up the closer structure and the further structure including the WBL 091 and PPS2 187 groups (White et al. 1999; Trasarti-Battistoni 1998).

## 6. CONCLUSIONS

One of the principle goals of the AGES is to investigate the population of dwarf galaxies in different environments. Our H I mapping of the NGC 7332 group

TABLE 6  
 OPTICAL IDENTIFICATIONS OF GALAXIES IN THE NGC 1156 AND NGC 7332 FIELDS.

AGES ID	R.A. (J2000)	Dec (J2000)	$\Delta\alpha$ (sec)	$\Delta\delta$ (arcsec)	$B_J$	$R$	$M_{HI}/L_B$ ( $M_\odot/L_\odot$ )	Literature Name	Velocity ( $\text{km s}^{-1}$ )
J025512+243812	02:55:12.49	24:38:05.9	-0.59	6.1	15.85	15.59	$0.14 \pm 0.05$	CGCG 484-024	6996
J025626+254614	02:56:27.73	25:46:18.6	-1.73	-4.6	20.29	19.38	$1.00 \pm 0.56$		
J025737+244321	02:57:38.56	24:43:20.1	-2.06	0.9	17.01	16.27	$0.48 \pm 0.16$	2MASX J02573860+2443194	
J025742+261755 <sup>a</sup>	02:57:41.98	26:16:37.2	0.42	77.8	18.78	18.04	$3.19 \pm 0.24$	AGC 122807	10370
J025753+255737 <sup>b</sup>	02:57:52.68	25:58:11.5	0.52	-34.5	17.08	16.69	$0.65 \pm 0.22$	2MASX J02575260+2558114	
J025801+252556 <sup>c</sup>	02:57:59.12	25:25:26.9	-1.70	29.1	16.05	15.50	$0.44 \pm 0.14$	CGCG 485-002B	6904
J025818+252711 <sup>d</sup>	02:58:18.23	25:26:54.9	-0.57	16.0	16.54	15.61	$0.63 \pm 0.20$	CGCG 485-004	10510
J025826+241836	02:58:22.35	24:18:24.4	3.24	11.6	18.01	16.97	$1.05 \pm 0.36$	2MASX J02582235+2418241	
J025835+241844	02:58:37.36	24:18:33.3	-2.56	10.7	17.21	16.66	$0.99 \pm 0.23$	2MASX J02583738+2418331	
J025836+251656 <sup>e</sup>	02:58:35.51	25:16:48.3	-0.01	7.6	16.05	15.14	$0.86 \pm 0.28$	UGC 02442	10452
J025842+252348 <sup>f</sup>	02:58:44.47	25:23:41.8	-2.27	6.2	16.19	15.24	$0.39 \pm 0.13$	V Zw 298	10375
J025843+254521	02:58:43.83	25:45:28.5	-1.23	-8.5	18.74	17.63	$3.4 \pm 1.1$	UGC 02445	7215
J025902+253518	02:59:00.29	25:35:12.7	1.51	6.3	18.31	17.34	$0.31 \pm 0.12$		
J025917+244756 <sup>g</sup>	02:59:17.48	24:48:43.1	-0.08	-47.1	19.80	19.29	$2.07 \pm 0.74$		
J025930+255419	02:59:31.58	25:54:12.3	-1.28	6.7	17.02	16.11	$0.33 \pm 0.11$	2MASX J02593158+2554122	
J025936+253446 <sup>h</sup>	02:59:34.97	25:35:02.5	1.03	-16.5	19.22	18.43	$0.55 \pm 0.22$		
J025942+251430 <sup>i</sup>	02:59:42.30	25:14:16.2	0.00	13.8	-	-	$0.32 \pm 0.06$	NGC 1156	375
J025953+254350 <sup>j</sup>	02:59:51.33	25:44:21.4	1.67	-31.4	20.43	18.32	$0.78 \pm 0.37$		
J025954+241323	02:59:54.98	24:13:30.6	-0.89	-7.6	16.25	14.75	$0.54 \pm 0.18$	UGC 02457	10217
J030008+241600	03:00:08.12	24:15:50.6	0.18	9.4	17.43	16.06	$0.74 \pm 0.28$	2MASX J03000813+2415503	
J030014+250315 <sup>k</sup>	03:00:13.88	25:03:25.6	0.12	-10.6	21.50	-	$11.1 \pm 3.8$		
J030025+255335	03:00:26.97	25:53:32.9	-2.07	2.0	22.41	20.58	$7.3 \pm 3.6$		
J030027+241301 <sup>l</sup>	03:00:21.98	24:12:50.6	5.22	10.4	18.63	17.88	$1.52 \pm 0.51$		
J030036+241156 <sup>m</sup>	03:00:38.69	24:12:22.9	-2.29	-26.9	19.05	18.45	$1.13 \pm 0.46$		
J030039+254656	03:00:38.71	25:47:01.3	0.59	-5.3	20.14	19.69	$0.62 \pm 0.26$		
J030112+242411	03:01:12.46	24:24:19.9	-0.96	-8.9	16.92	15.58	$0.62 \pm 0.20$	2MFGC 02447	
J030136+245602 <sup>n</sup>	03:01:37.68	24:55:34.4	-1.58	27.6	17.96	17.12	$0.24 \pm 0.09$		
J030139+254442	03:01:39.68	25:44:16.5	-0.47	25.5	18.92	18.37	$2.27 \pm 0.75$		
J030146+254314 <sup>o</sup>	03:01:43.56	25:42:46.5	2.24	27.5	17.17	16.02	$0.66 \pm 0.22$	2MASX J03014354+2542474	
J030200+250030	03:02:00.32	25:00:52.3	-0.62	-22.3	17.68	16.65	$0.86 \pm 0.28$	2MASX J03020033+2500524	
J030204+254745	03:02:04.30	25:47:35.5	-0.30	9.5	17.16	15.86	$0.67 \pm 0.22$	FGC 0378	6786
J030234+244938	03:02:34.20	24:49:48.9	-0.10	-10.9	20.03	18.07	$4.3 \pm 1.4$		
J030254+260028	03:02:54.43	26:00:24.3	-0.23	3.7	18.33	17.37	$2.01 \pm 0.66$	LSBC F480-V04	10618
J030309+260407	03:03:08.92	26:03:35.5	-0.32	31.5	18.41	17.90	$0.63 \pm 0.23$		
J030325+241510 <sup>p</sup>	03:03:27.46	24:15:05.3	-2.86	4.7	16.78	15.81	$0.33 \pm 0.11$		
J030355+241922	03:03:53.63	24:19:24.4	1.08	-2.4	19.56	18.94	$2.23 \pm 0.79$		
J030450+260045	03:04:49.57	26:01:15.8	0.73	-30.9	19.37	18.39	$0.88 \pm 0.39$		
J030453+251532	03:04:55.12	25:15:56.1	-2.02	-24.1	17.81	17.07	$0.60 \pm 0.21$	2MASX J03045528+2515558	

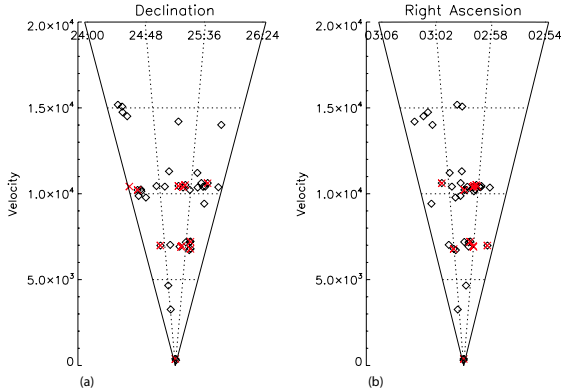


FIG. 17.— Pie-slices of the large scale structure in the region behind NGC 1156: (a) Declination; (b) Right Ascension. Literature galaxies (with redshifts) are shown as red crosses; AGES galaxies are shown as black diamonds. The horizontal axis has been expanded for clarity.

has revealed two new dwarf members, doubling the number of confirmed group members. An additional possible member has been found in an optical search, bringing the number of possible dSph companions without redshift information to three and the total number of possible galaxies in the group to seven. In the NGC 1156 group, we found a single dwarf companion that had not

been previously catalogued. This does not appear to be large enough or currently close enough to NGC 1156 to have a significant effect on that galaxy.

In the background regions, we have detected 82 sources, 45 of which are entirely new discoveries. We find evidence of large scale structure in both cubes, with newly-discovered structures at  $\sim 12000$  and  $\sim 16000$   $\text{km s}^{-1}$  behind NGC 7332 and confirm structures visible in the literature redshifts at  $\sim 7000$  and  $\sim 10000$   $\text{km s}^{-1}$  behind NGC 7332. We also find one galaxy in the void region between 2000 and 7000  $\text{km s}^{-1}$  behind NGC 7332.

#### ACKNOWLEDGEMENTS

We thank Mike Irwin for keeping the archive of the APM surveys available, Mark Calabretta and the ATNF for maintaining the Livedata and Gridzilla multibeam processing packages and for modifying them to read Arecibo data and Giuseppe Gavazzi and Luca Cortese for useful discussions and the optical spectroscopy observations presented in Section 4.3. We also thank the anonymous referee for his useful comments that helped improve the paper.

I.D.K. was partially supported by RFBR grants 10-02-00123 and RUS-UKR 09-02-90414.

This research is partly based on observations obtained at the Canda-France-Hawaii Telescope (CFHT) which is

TABLE 6  
(CONTINUED)

AGES ID	R.A. (J2000)	Dec (J2000)	$\Delta\alpha$ (sec)	$\Delta\delta$ (arcsec)	$B_J$	$R$	$M_{HI}/L_B$ ( $M_\odot/L_\odot$ )	Literature Name	Velocity ( $\text{km s}^{-1}$ )
J223111+234146	22:31:11.09	23:41:17.2	-0.09	28.7	18.15	17.13	$1.14 \pm 0.42$		
J223122+230436	22:31:21.98	23:04:41.0	0.13	-5.0	16.77	15.97	$0.45 \pm 0.16$	2MASX J22312197+2304404	
J223143+244513	22:31:43.36	24:44:58.0	-0.36	15.7	16.02	14.91	$0.18 \pm 0.06$	MCG +04-53-003	
J223213+232657	22:32:13.17	23:26:58.1	-0.57	-1.1	16.76	15.92	$0.79 \pm 0.26$	2MASX J22321321+2326574	
J223218+235131 <sup>q</sup>	22:32:19.88	23:51:48.7	-2.08	-17.7	15.98	15.11	$0.23 \pm 0.08$	CGCG 474-005	11947
J223223+232613	22:32:20.82	23:26:51.3	2.58	-38.3	18.84	17.87	$3.2 \pm 1.1$		
J223231+231601	22:32:31.98	23:16:37.6	-1.48	-36.6	15.80	11.03	$0.24 \pm 0.08$	KUG 2230+230	11782
J223236+235555	22:32:36.55	23:55:54.4	-0.25	0.5	16.41	15.43	$1.21 \pm 0.39$	UGC 12072	7454
J223237+231209 <sup>f</sup>	22:32:37.59	23:12:39.9	-0.39	-30.9	17.23	16.63	$0.44 \pm 0.16$		
J223245+243816	22:32:44.30	24:38:41.4	0.90	-25.4	17.98	18.15	$0.53 \pm 0.21$		
J223318+244545	22:33:16.60	24:45:41.1	1.19	3.9	16.76	15.75	$0.62 \pm 0.32$	2MASX J22331661+2445408	
J223320+230400	22:33:20.29	23:04:00.2	-0.09	-0.2	19.52	18.72	$4.0 \pm 1.4$		
J223329+231109	22:33:27.31	23:10:29.2	1.79	39.8	17.51	16.87	$1.22 \pm 0.41$		
J223342+242712	22:33:37.42	24:26:34.0	4.68	38.0	17.49	16.92	$0.87 \pm 0.30$		
J223355+243114	22:33:58.23	24:32:25.6	-3.33	-71.6	19.20	18.29	$1.63 \pm 0.63$		
J223415+233057	22:34:18.28	23:31:00.2	-3.28	-3.2	17.07	17.11	$0.32 \pm 0.12$		
J223449+240744	22:34:49.68	24:07:55.5	-0.88	-11.5	17.35	16.71	$0.35 \pm 0.13$		
J223502+235258 <sup>s</sup>	22:35:00.25	23:53:02.5	1.45	-4.5	17.61	16.51	$0.36 \pm 0.15$		
J223502+242131 <sup>t</sup>	22:35:01.51	24:20:31.0	0.89	60.0	19.09	18.04	$1.88 \pm 0.71$		
J223506+233707	22:35:06.15	23:37:12.5	-0.55	-5.5	19.00	18.51	$3.9 \pm 1.3$		
J223517+244317 <sup>u</sup>	22:35:14.88	24:43:26.7	1.91	-9.7	17.93	17.17	$0.47 \pm 0.25$		
J223605+242407 <sup>v</sup>	22:36:02.40	24:24:12.0	2.30	-5.0	17.93	16.67	$0.26 \pm 0.10$		
	22:36:03.47	24:24:08.7	1.23	-1.7	18.03	16.97	$0.26 \pm 0.10$		
J223613+243504	22:36:13.39	24:34:59.5	-0.39	4.5	16.75	15.31	$0.76 \pm 0.25$	2MASX J22361331+2434596	
J223627+234258	22:36:27.85	23:42:59.4	-0.65	-1.4	17.04	15.94	$0.45 \pm 0.15$		
J223628+245307	22:36:30.28	24:52:23.2	-2.48	43.8	19.29	-	$5.2 \pm 2.1$		
J223631+240823	22:46:31.28	24:08:14.9	-0.68	8.1	19.72	18.27	$3.6 \pm 1.3$		
J223701+225532	22:36:59.83	22:55:39.3	0.97	-7.3	17.95	17.88	$2.25 \pm 0.74$	KUG 2234+226	11511
J223715+232957	22:37:15.19	23:29:38.1	-0.19	18.9	17.62	16.76	$0.48 \pm 0.19$		
J223739+244947	22:37:38.28	24:49:30.1	0.82	16.9	17.73	16.34	$1.59 \pm 0.54$		
J223741+242520	22:37:41.12	24:25:28.2	-0.12	-8.2	18.57	18.13	$3.66 \pm 1.19$		
J223745+225309 <sup>w</sup>	22:37:48.49	22:52:53.8	-3.49	15.2	21.39	19.37	$11.3 \pm 4.5$		
J223746+234712	22:37:47.24	23:47:12.1	-0.74	-0.1	13.50	11.60	$0.30 \pm 0.10$	NGC 7339	1313
J223823+245207 <sup>x</sup>	22:38:26.39	24:51:14.4	3.01	20.6	17.52	16.22	$0.71 \pm 0.30$		
J223829+235135	22:38:29.69	23:51:31.4	-0.29	3.6	19.95	-	$4.3 \pm 1.5$		
J223834+231114	22:38:34.56	23:11:11.7	-0.16	2.2	18.24	16.93	$1.82 \pm 0.65$		
J223839+234247 <sup>y</sup>	22:38:39.38	23:42:49.9	-0.38	-2.9	17.89	16.26	$0.79 \pm 0.29$		
J223842+233156	22:38:43.20	23:32:08.9	-0.90	-12.9	18.13	16.91	$1.60 \pm 0.55$		
J223846+234923	22:38:47.02	23:49:45.5	-1.42	-22.5	19.56	18.76	$3.8 \pm 1.4$		
J223900+244752	22:38:59.75	24:47:57.3	0.35	-5.3	16.75	15.11	$0.61 \pm 0.21$	2MASX J22385968+2447579	
J223905+240651	22:39:05.23	24:06:53.8	-0.13	-2.8	17.86	16.48	$1.85 \pm 0.61$		
J223946+242157 <sup>z</sup>	22:39:47.20	24:22:42.6	-0.90	45.6	17.12	15.45	$0.32 \pm 0.11$	2MASX J22394715+2422428	
J224005+244154	22:40:05.97	24:41:53.6	-1.37	0.4	16.50	14.94	$1.99 \pm 0.49$	NSF J224006.18+244157.1	11992
J224016+244658	22:40:16.69	24:46:54.1	-0.39	3.9	16.62	15.22	$0.14 \pm 0.06$	2MASX J22401669+2446537	
J224024+243019	22:40:25.38	24:30:16.5	-1.38	2.5	19.08	17.85	$1.17 \pm 0.46$		
J224025+243925	22:40:28.19	24:40:05.3	-3.28	-40.3	16.68	15.07	$0.32 \pm 0.12$	2MASX J22402816+2440055	
J224039+243229	22:40:39.16	24:32:29.5	-0.16	-0.5	18.77	18.06	$1.74 \pm 0.63$		
J224052+234635	22:40:52.34	23:46:29.3	-0.01	5.3	19.37	19.01	$2.36 \pm 0.88$		
J224110+243500	22:41:09.47	24:34:28.7	0.43	-31.3	18.22	16.87	$4.54 \pm 1.49$		
J224125+232228	22:41:24.59	23:22:28.7	0.91	-0.7	14.95	14.09	$0.22 \pm 0.07$	IC 5243	7144

operated by the National Research Council of Canada, the Institut National des Sciences de l'Univers of the Centre National de la Recherche Scientifique of France, and the University of Hawaii.

This research has made use of data obtained from the SuperCOSMOS Science Archive, prepared and hosted by the Wide Field Astronomy Unit, Institute for Astronomy, University of Edinburgh, which is funded by the UK Science and Technology Facilities Council.

## REFERENCES

- Aldering G. et al., 2007, Central Bureau Electronic Telegram, 991  
 Ajhar E. A., Lauer T. R., Tonry J. L., Blakeslee J. P., Dressler A., Holtzman J. A., Postman M., 1997, AJ, 114, 626  
 Auld R. et al., 2006, MNRAS, 371, 1617  
 Balkowski C., Chamaraux P., 1983, A&AS, 51, 331  
 Barazza F. D., Binggelli B., Prugniel P., 2001, A&A, 373, 12  
 Barnes D. G. et al., 2001, MNRAS, 322, 486  
 Biermann P., Clarke J. N., Fricke K. J., 1979, A&A, 75, 19  
 Burstein D., Krumm N., Salpeter E. E., 1987, AJ, 94, 88  
 Condon J., Cotton W. D., Greisen E. W., Yin Q. F., Perley R. A., Taylor G. B., Broderick J. J., 1998, AJ, 115, 1693  
 Cortese L. et al., 2008, MNRAS, 383, 1519  
 De Vaucouleurs G., de Vaucouleurs A., Corwin H. G., But R. J., Paturel G., Fouque P., 1991, "Third Reference Catalogue of Bright Galaxies", Springer-Verlag, New York.  
 Disney M. J., Phillips S., 1983, MNRAS, 205, 1253  
 Fairall A. P., 1998, "Large Scale Structures in the Universe", Wiley, New York.  
 Falc3n-Barroso J. et al., 2004, MNRAS, 350, 35  
 Giovanelli R. et al., 2005, AJ, 130, 2613  
 Gregory S. A., Tift W. G., Moody J. W., Newberry M. V., Hall S. M., 2000, AJ, 119, 545



TABLE 6  
(CONTINUED)

- <sup>a</sup> Fainter galaxy closer at 02:57:43.6, 26:17:54 with  $B_J = 21.3$ .  
<sup>b</sup> Fainter galaxy closer at 02:47:53.0, 25:57:34 with  $B_J = 19.7$ .  
<sup>c</sup> CGCG 484-026 at  $6966 \text{ km s}^{-1}$  also lies within the beam at 02:58:03.2, 25:26:57 with  $B_J = 14.5$ . Spectrum appears to show two distinct components, consistent with two confused galaxies.  
<sup>d</sup> CFHT observations give  $g = 14.52 \pm 0.02$ ,  $r = 14.87 \pm 0.02$ .  
<sup>e</sup> CFHT observations give  $g = 15.04 \pm 0.02$ ,  $r = 14.76 \pm 0.02$ .  
<sup>f</sup> CFHT observations give  $g = 15.09 \pm 0.02$ ,  $r = 14.59 \pm 0.02$ .  
<sup>g</sup> CFHT observations give  $g = 18.31 \pm 0.03$ ,  $r = 18.03 \pm 0.03$ . Fainter galaxy closer at 02:59:16.4, 24:48:30 with  $B_J = 20.4$ , and other faint galaxies in the vicinity.  
<sup>h</sup> CFHT observations give  $g = 17.99 \pm 0.02$ ,  $r = 17.76 \pm 0.02$ .  
<sup>i</sup> Too bright for SuperCOSMOS photometry, RC3 value of  $12.08 \pm 0.16$  used to calculate  $M_{HI}/L_B$ .  
<sup>j</sup> Fainter galaxy closer at 02:59:53.8, 25:43:58 with  $B_J = 22.5$ .  
<sup>k</sup> CFHT observations give  $g = 19.19 \pm 0.03$ ,  $r = 18.87 \pm 0.03$ .  
<sup>l</sup> Fainter galaxy closer at 03:00:25.6, +24:13:13 with  $B_J = 20.9$ , and other even fainter galaxies closer than this.  
<sup>m</sup> Fainter galaxy closer at 03:00:37.3, +24:11:44 with  $B_J = 22.5$ .  
<sup>n</sup> CFHT observations give  $g = 17.24 \pm 0.02$ ,  $r = 16.60 \pm 0.02$ . Fainter galaxy closer at 03:01:37.2, +24:56:13 with  $B_J = 20.8$ .  
<sup>o</sup> CFHT observations give  $g = 15.85 \pm 0.02$ ,  $r = 15.37 \pm 0.02$ .  
<sup>p</sup> May have star superposed. Some much fainter galaxies lie closer.  
<sup>q</sup> A similar galaxy is found at 22:32:38.5 +23:11:41 with  $B_J = 18.3$ .  
<sup>r</sup> Elongated image at 22:35:02.7 +23:52:55 with  $B_J = 22.6$ .  
<sup>s</sup> May have star superposed. Some much fainter galaxies lie closer.  
<sup>t</sup> Smaller and fainter galaxies at 22:35:04.4, +24:21:57 with  $B_J = 20.9$  and at 22:35:17.5 +24:43:31 with  $B_J = 19.83$ .  
<sup>u</sup> An elongated compact object lies at 22:38:29.65 +23:51:34.5,  $B_J=19.75$ ,  $R=17.63$ ,  $I=17.15$   
<sup>v</sup> Pair of interacting galaxies.  $M_{HI}/L_B$  is average for the pair.  
<sup>w</sup> Multiple faint galaxies in the region.  
<sup>x</sup> Fainter galaxy closer at 22:38:23.1, +24:51:56 with  $B_J = 21.4$ .  
<sup>y</sup> Fainter galaxy closer at 22:38:39.0, +23:42:56 with  $R = 20.8$ .  
<sup>z</sup> Fainter galaxy closer at 22:39:46.9, +24:21:33 with  $B_J = 21.63$ .

TABLE 7  
LITERATURE REDSHIFTS FOR GALAXIES IN THE VOLUME BEHIND NGC 1156  
AND NGC 7332

ID	Redshift ( $\text{km s}^{-1}$ )	Reference
CGCG 484-024	6996	Springob et al. 2005
AGC 122807	10370	Saintonge et al. 2008
CGCG 485-002B	6904	Springob et al. 2005
CGCG 484-026	7003	Springob et al. 2005
CGCG 485-003	10429	Springob et al. 2005
CGCG 485-004	10510	Springob et al. 2005
UGC 02442	10452	Springob et al. 2005
UGC 02445	7215	Springob et al. 2005
V Zw 298	10375	Springob et al. 2005
UGC 02457	10217	Springob et al. 2005
FGC 0378	6786	Springob et al. 2005
LSBC F480-V04	10618	Saintonge et al. 2008
CGCG 474-005	11947	Springob et al. 2005
KUG 2230+230	11782	Springob et al. 2005
UGC 12072	7454	Springob et al. 2005
2MASX J22335064+2426393	10103	Lawrence et al. 1999
IC 5231	7473	Gregory et al. 2000
KUG 2234+226	11511	Springob et al. 2005
NSF J224006.18+244157.1	11992	Aldering et al. 2007
IC 5242	7145	Springob et al. 2005
IC 5243	7154	Springob et al. 2005

Grossi M., Disney M. J., Pritzl B. J., Knezek P. M., Gallagher J. S., Minchin R. F., Freeman, K. C., 2007, MNRAS, 374, 107  
Hambly N. C., Irwin M. J., MacGillivray H. T., 2001, MNRAS, 326, 1295  
Haynes M. P., 1981, AJ, 86, 1126  
Haynes, M. P., van Zee, L., Hogg, D. E., Roberts, M. S., Maddalena, R. J., 1998, AJ, 115, 62  
Henning P. A. et al. 2010, AJ, 139, 2130  
Helou G., Soifer B. T., Rowan-Robinson M., 1985, ApJ, 298, L7  
Huchtmeier W. K., Karachentsev I. D., Karachentseva V. E., 2000, A&AS, 147, 187

Hunter D. A., Rubin V. C., Swaters R. A., Sparke L. S., Levine S. E., 2002, ApJ, 580, 194  
James P. A. et al., 2004, A&A, 414, 23  
Karachentseva V. E., Lebedev V. S., Shcherbanovskij A. L., 1973, Communications of the Special Astrophysical Observatory of the USSR AS, No. 8.  
Karachentseva V. E., Karachentsev I. D., Richter G. M., 1999, A&AS, 135, 221  
Karachentsev I., Musella I., Grimaldi A., 1996, A&A, 310, 722  
Kent B. R., Spekkens K., Giovanelli R., Haynes M. P., Momjian E., Cortes J. R., Hardy E., West A., 2009, ApJ, 691, 1595  
Knapp G. R., Kerr F. J., Williams B. A., 1978, ApJ, 222, 800

- Koribalski B. S. et al., 2004, *AJ*, 128, 16  
Lawrence A. et al., 1999, *MNRAS*, 308, 897  
Morganti R. et al., 2006, *MNRAS*, 371, 157  
Moshir M. et al., 1990, "IRAS Faint Source Catalog, Version 2.0"  
Plana H., Boulesteix J., 1996, *A&A*, 307, 391  
Putman M. E. et al., 2002, *AJ*, 123, 873  
Saintonge A., Giovanelli R., Haynes M., Hoffman, G. L., Kent B. R., Martin A. M., Stierwalt S., Brosch N. , 2008, *AJ*, 135, 588  
Schlegel D. J., Finkbeiner D. P., Davis M., 1998, *ApJ*, 500, 525  
Simien F., Prugniel Ph., 1997, *A&AS*, 126, 519  
Springob C. M., Haynes M. P., Giovanelli R., Kent B. R., 2005, *ApJS*, 160, 149  
Tully R. B., Fisher J. R., 1988, *Catalog of Nearby Galaxies*, CUP, Cambridge  
Staveley-Smith L., Davies R. D., 1987, *MNRAS*, 224, 953  
Swaters R. A., van Albada T. S., van der Hulst J. M., Sancisi R., 2002, *A&A*, 390, 829  
Tonry J. L. et al., 2001, *ApJ*, 546, 681  
Trasarti-Battistoni R., 1998, *A&AS*, 130, 341  
Verley S., Leon S., Verdes-Montenegro L., Combes F., Sabater J., Sulentic J., Bergond G., Espada D., García E., Lisenfeld U., Odewahn S. C., 2007, *A&A*, 472, 121  
White R. A., Bliton M., Bhavsar S. P., Bornmann P., Burns J. O., Ledlow M. J., Loken C., 1999, *AJ*, 118, 2014  
Yun M. S., Reddy N. A., Condon J. J., 2001, *ApJ*, 554, 803  
Zwaan M. A., Meyer M. J., Staveley-Smith L., Webster R. L., 2005, *MNRAS*, 359, 30L